The Coulon deposit: quantifying alteration in VMS systems modified by amphibolite facies metamorphism

Lucie Mathieu*, Rose-Anne Bouchard, Vital Pearson, and Réal Daigneault

L. Mathieu. CONSOREM (Consortium de Recherche en Exploration Minérale - Mineral exploration research consortium), 555 Boul. de l'Université, Chicoutimi, Canada, G7H 2B1 (e-mail: mathiel@tcd.ie).

R.A. Bouchard, R. Daigneault. Centre d'études sur les Ressources minérales (CERM) - Université du Québec à Chicoutimi, 555 Boul. de l'Université, Chicoutimi, Canada, G7H 2B1. (e-mail: rose-anne.bouchard@uqac.ca; Real_Daigneault@uqac.ca).

V. Pearson. Redevance Aurifères Osisko Ltd., Exploration Osisko Baie James – 300 rue Saint-Paul (office 200), Québec, Québec, G1K 7R1 (e-mail: vpearson@osiskogr.com).

***Corresponding author:** Lucie Mathieu (e-mail: mathiel@tcd.ie; tel: 1-418-545-5011 ext. 2538)

Abstract: The Coulon deposit is a volcanogenic massive sulphide (VMS) system in the James Bay area, Superior Craton, Québec, that was metamorphosed to amphibolite-facies conditions. The chemistry and mineralogy of the VMS-related alteration halo proximal to the mineralised sulphide lenses are investigated, using samples collected in the field and 5583 chemical analyses provided by Osisko Ltd. Alteration is quantified using mass balance and normative calculations, and the application and performance of these methods in an exploration context are investigated. In VMS systems, altered rocks proximal to the ore zones are characterised by multi-element metasomatism, which is best quantified by mass balance methods that have been successfully applied in the study area. However, mass balance calculations necessitate the documentation of a precursor, which is not always possible in an exploration context; therefore an alternative method (i.e. alteration indices) was also evaluated. In most VMS systems, proximal alteration is characterised by chlorite (chloritisation), muscovite (sericitisation), and quartz (silicification) while, at the Coulon deposit, altered rocks contain mostly cordierite, biotite, sillimanite, and quartz. Alteration indices were calculated using observed and normative minerals, and provide satisfactory results similar to those obtained with mass balance calculations. Using these results, recommendations are made to estimate the intensity of alteration in the core shack using the proportions of observed minerals. Alteration indices are sensitive to the composition of precursors and, due to high grade metamorphism, chloritisation and sericitisation are not precisely quantified. Recognising these limitations is essential to successful quantification of alteration in areas metamorphosed to high-grade conditions.

Keywords: Coulon VMS, hydrothermal alteration, CONSONORM, alteration indices, mass balance.

Résumé : Le dépôt de Coulon est un sulfure massif volcanogène (SMV) situé à la Baie James, Craton du Supérieur, Québec, qui a été métamorphisé dans les conditions du facies des amphibolites. La chimie et la minéralogie de la partie du halo d'altération de ce SMV située à proximité des lentilles minéralisées sont étudiées à partir d'échantillons collectés sur le terrain et de 5583 analyses chimiques appartenant à Osisko Inc. L'altération est quantifiée avec des calculs normatifs et de bilans de masse, et la performance et la pertinence de ces méthodes dans un contexte d'exploration sont étudiées. Dans les systèmes de SMV, les roches altérées proximales aux zones minéralisées sont caractérisées par un métasomatisme multiélément qui peut être quantifié précisément par des méthodes de type bilans de masse, qui ont été appliquées avec succès dans la zone étudiée. Cependant, les calculs de bilans de masse nécessitent la documentation d'un précurseur, ce qui n'est pas toujours possible dans un contexte d'exploration ; et c'est pourquoi une méthode alternative (c.-à-d. indices d'altération) a également été testée. Dans la plupart des systèmes SMV, l'altération proximale est caractérisée par chlorite (chloritisation), muscovite (sericitisation), et quartz (silicification) tandis que, pour le dépôt de Coulon, les roches altérées contiennent principalement cordiérite, biotite, sillimanite, et quartz. Les indices d'altération ont été calculés à partir de minéraux observés et normatifs, et procurent des résultats satisfaisants similaires à ceux obtenus avec les calculs de bilans de masse. A partir de ces résultats, des recommandations sont formulées qui permettront d'estimer l'intensité de l'altération

dans la carothèque à partir des proportions des minéraux observés. Les indices d'altération sont sensibles à la composition des précurseurs et, à cause du métamorphisme de haut grade, la chloritisation et la séricitisation ne peuvent pas être précisément quantifiées. Reconnaitre ces limites est essentiel à une quantification correcte de l'altération dans des zones métamorphisées dans des conditions de haut-grade.

Mots clés: SMV de Coulon, altération hydrothermale, CONSONORM, indices d'altération, bilans de masse.

Introduction

The quantification of alteration associated with volcanogenic massive sulphide (VMS) systems is important to understanding alteration processes and is essential to targeting mineralisation during exploration. To quantify alteration, numerous chemical methods exist, the practicality of which depends on the nature of precursors, on the level of documentation, and on the characteristics of the available chemical data. The advantages and limitations of these methods are well documented in typical VMS settings (e.g. Leitch and Lentz 1994) but not in areas that have been subjected to high-grade metamorphism. Metamorphism may re-crystallise, devolatilise, and partially melt alteration halos enriched in potassium and water (e.g. Katz 1988; Gauthier 2000; Tomkins 2007), and such processes may impair alteration quantification. In this contribution, the performance of two chemical methods will be evaluated using the example of the Coulon VMS deposit, which was metamorphosed at amphibolite-facies conditions.

The alteration halos of VMS systems are well documented and characterised by the following alteration styles: 1) distal epidotisation, which forms quartz-epidote veins; 2) carbonatization, which is variable in its intensity and distribution; and proximal 3) sericitisation (acidic alteration inducing feldspar destruction); 4) chloritisation; and 5) silicification (Franklin et al. 2005; Hannington et al. 2005; Galley et al. 2007). Such alteration corresponds to distal Ca-Si-metasomatism, and proximal K-, Na-, Ca-, Fe-, Mg-, and Si-metasomatism, respectively. Most VMS systems display low-grade assemblages dominated by chlorite, muscovite, and quartz (e.g. Galley et al. 2007). When metamorphosed to amphibolite-facies conditions, proximal assemblages are characterised

by cordierite, anthophyllite, biotite, quartz, and sillimanite (e.g. Montauban and Noranda VMS; Prabhu and Webber 1984; Bernier and MacLean 1993; Liaghat and MacLean 1995). Such assemblages are abundantly described for metamorphic rocks with altered protoliths (e.g. Riverin and Hodgson 1980; Pan and Fleet 1995; Tiwary and Deb 1997; Bonnet et al. 2005; Peck and Smith 2005; Bonnet and Corriveau 2007; Zheng et al. 2011).

In general, metasomatism is best quantified by mass balance calculations (e.g. Grant 1986; Leitch and Day 1990; MacLean and Barrett 1993). Such methods are little used in the context of exploration, possibly because they are viewed as complex mathematical models and require the documentation of immobile elements and precursors. In poorly documented areas, the identification of least-altered rocks, for example, can be challenging; hence the necessity of developing alternative methods. Alteration indices calculated using ratios of major elements have been used (e.g. Ishikawa et al. 1976), but are strongly sensitive to the composition of precursors (e.g. Trépanier et al. 2015) and will not be discussed further in this contribution. Alternatively, alteration indices can be calculated using the proportions of minerals observed in thin sections or, as is more often feasible in exploration contexts, that have been calculated using normative solutions such as early calculations (Barth 1959; Riverin and Hodgson 1980), NORMAT (Piché and Jébrak 2004), CONSONORM_LG (Trépanier et al. 2015) or CONSONORM_HG (Mathieu et al. 2016).

The Coulon deposit has been documented and sampled by Osisko Exploration Baie James (Osisko Ltd.), and mineralogical data as well as abundant geochemical data are available (unpublished data from Osisko Ltd.). This dataset will form the basis for

this study in which mass balance and normative calculations will be performed. A comparison of these methods, their sensitivity to metamorphic processes, and their applicability to the exploration industry will then be discussed.

Geological setting

The Coulon deposit is an Archean VMS system in the James Bay area of Québec, Canada. It is owned and explored by Osisko Ltd. A regional study of the area was performed by the ministère de l'énergie et des ressources naturelles (MERN) of Québec (Gosselin and Simard 2001; Thériault and Chevé 2001), and local mineral assessments were completed by Osisko Ltd. (Tracy et al. 2009; Savard et al. 2013).

The deposit occurs within the ca. 2873 Ma Coulon greenstone belt of the La Grande Subprovince, Superior craton (David et al. 2009) (Fig. 1a). The belt has a strike length of 50 km and is dominated by mafic to locally felsic metavolcanic and minor metasedimentary rocks of the Gayot Complex and metasedimentary rocks of the Aubert Formation (Gosselin and Simard 2001; Thériault and Chevé 2001) (Fig. 1b). Felsic intrusions in the area include the Brésolles suite (gneissic basement to the greenstone belt), as well as granodiorite of the ca. 2700 Ma Maurel suite and granite of the Tramont suite (David et al. 2009; Savard et al. 2013).

Eight massive sulphides lenses of mineralisation occur in the felsic lithologies of the Gayot complex (Fig. 1b). These lithologies, in the mineralised areas, are dominated by metavolcanic rocks (see section "Nature of precursors"). Most lenses are located at the folded, locally sub-vertical, lithological contact between mafic and felsic units, and are adjacent to stringer zones that, prior to deformation, likely underlied the lenses. The

lenses contain mostly pyrrhotite, pyrite, sphalerite, chalcopyrite, and galena (Savard et al. 2013). In the following, we will address the alteration associated with the "Main Area" (i.e. lenses 44, 08, 9-25, and 16-17), which currently contains an indicated resource of 3.7 Mt at 3.59% Zn, 1.27% Cu, 0.4 % Pb, 37.04 g/t Ag and 0.25 g/t Au, with an additional inferred resource of 10.1 Mt (Tracy et al. 2009).

The Coulon greenstone belt and deposit were deformed and re-crystallised under amphibolite-facies conditions (Simard et al. 2010). The Coulon deposit's massive sulphide lenses are elongate and tabular: lenses 08 and 9-25 (Fig. 1b), for example, have horizontal extents of about 300 m, vertical extents of ~700 m, and thicknesses of 10 to 30 m. Such high aspect ratios were likely acquired during deformation. The lenses also display imbricated "J-shape" geometries that result from structural duplication and folding (Savard et al. 2013). Migmatites are abundant in the greenstone belt, including the Coulon deposit area, except within the Main Area where only local occurrences are reported (Savard et al. 2013).

In the following, the chemistry and mineralogy of rocks proximal to the mineralised Main Area will be investigated.

Methodology

Alteration styles at Coulon are quantified using 5583 unpublished bulk-rock geochemical analyses of drill core samples from Osisko Ltd. The samples were decomposed by lithium meta- or tetraborate fusion, and then analysed at the ALS-Chemex laboratory by X-ray fluorescence for SiO_2, TiO_2, Al_2O_3, FeO_T, MgO, MnO, CaO, Na_2O, K_2O, P_2O_5, LOI, Cr, Ba, Sr, Y, and Zr (Table 1). The detection limits are

0.01 wt% for most elements, except for Y and Zr (2 ppm) (Savard et al. 2013, pp. 49-51). Rigorous quality assurance-quality control (QA-QC) procedures were maintained, including the use of blanks, standards and duplicates (Savard et al. 2013, pp. 51-53).

Mineral assemblages are documented using field investigations, which were undertaken in the vicinity of the mineralised areas, where rocks have dominantly mafic to felsic volcanic precursors (Savard et al. 2013). Field work was carried-out during the summer of 2013 by R.A. Bouchard in the Main Area (Fig. 1b) and a total of 38 standard thin sections were produced from samples collected in the field.

Nature of precursors

The rocks hosting VMS-type deposits have either sedimentary or igneous origins (Franklin et al. 2005; Hannington et al. 2005; Galley et al. 2007). At Coulon, the igneous (more specifically, volcanic) nature of the rocks hosting the mineralisation was confirmed using stratigraphic and textural observations (Savard et al. 2013). The Chemical Index of Alteration (CIA), which is a measure of weathering intensity (Nesbitt and Young 1984, 1989), has also been applied to rule out a sedimentary origin (Savard et al. 2013).

The samples of the Osisko dataset have then been chemically classified as altered rhyolite, dacite, andesite, and basalt (Savard et al. 2013). This classification, which could not be performed in the core shack due to alteration and metamorphism, relies on Zr/Ti ratios (MacLean and Barrett 1993) that are proxy to the SiO_2 content of igneous rocks (Winchester and Floyd 1977). These data, from the Coulon deposit, are compared to un-altered volcanic rocks from the pre-compiled files for rhyolite, dacite, andesite, and calc-alkaline to tholeiitic basalt of the GEOROC database (Sarbas 2008; GEOROC 2016).

Only GEOROC data with the following characteristics were considered: 1) majors, and Cr, Ba, Zr, Y are analysed; 2) loss on ignition (LOI) is < 3 wt% (to avoid possibly altered samples); and 3) rocks are designated as subaerial and volcanic. The GEOROC analyses have been averaged (Table 2) and compared to the mean values of the Coulon samples (Table 1; Fig. 2).

Most discrepancies are observed for rhyolites (see Sr and major elements; Fig. 2a) and are likely a consequence of alteration. Dacite, andesite, and basalt from Coulon are comparable to GEOROC's samples (Fig. 2b, c, d), and the differences observed for the mobile elements MgO, CaO, and Sr are likely due to alteration. Discrepancies are also observed for Cr, which is usually immobile during alteration (e.g. Hastie et al. 2007) and, consequently, Cr will not be used to calculate mass balance (see section "Method 1: mass balance calculations"). Correlation coefficients between averaged compositions of Coulon's altered rhyolite (Table 1) and of GEOROC's rhyolite, dacite, andesite, and basalt (Table 2) are 0.97, 0.83, 0.69, and 0.58, respectively; supporting the effectiveness of Zr/Ti ratios in classifying the altered rhyolite at Coulon.

Nature of least-altered felsic protoliths

The Coulon deposit is dominantly hosted by felsic metavolcanic units mostly classified as altered rhyolite (see previous section). In the field, distal to the mineralisation, sillimanite-bearing schist is observed that was initially viewed as the least-altered rhyolite unit and a possible equivalent to a precursor composition (i.e. unaltered protolith). To document the Al_2O_3-content of this unit, the incomplete mineral assemblage observations available in the Osisko database are used to identify 846 altered

rhyolites that contain >5 vol% sillimanite. These rocks have aluminium saturation index (ASI) >1 (Shand 1943), with mean, Q1 and Q3 (quartiles 1 and 3, or 25th and 75th centiles) values of 2.38, 1.34, and 3.01, respectively.

If the sillimanite-bearing schist is the least-altered part of the felsic metavolcanic unit, then it has either been strongly modified by sedimentary processes, which was ruled out using the CIA method (see previous section), or it has a strongly peraluminous precursor, which is difficult to reconcile with Coulon's geodynamic context. More likely, the sillimanite-bearing schist has an altered protolith; i.e. a felsic rock modified by acidic alteration that induced major elements leaching (Si excepted) and relative Al enrichment (e.g. Corriveau and Spry 2014).

As least-altered precursors could not be identified in the field or in the Osisko dataset, precursor compositions have been modelled (see next section).

Method 1: mass balance calculations

Mass balance calculations provide numerical estimates of the amount of major elements lost and gained during an alteration process by comparing the composition of an altered sample to that of its precursor. Mass balance methods are numerous (e.g. Barrett and MacLean 1994; Grant 1986) and are based upon the equations of mass transfers (Gresens 1967; Leitch and Lentz 1994). Such methods necessitate: 1) good quality analyses of the elements identified as immobile (e.g. Al_2O_3, TiO_2, Cr, Zr, Y, Nb, Th); and 2) the chemical composition of the precursor, which is usually interpreted as being the least-altered rock that could be identified in the field.

Reliable trace elements analyses are available from the Osisko database. However, this dataset lacks mineralogical or other information that would enable the identification of the least-altered samples. The composition of precursors has been modelled using the immobile elements Al_2O_3, TiO_2, Zr, and Y, and Trépanier's procedure (Trépanier et al. 2016), which consists of predicting the composition of a precursor for each sample and then using the equation of Grant (1986, 2005) to subsequently calculate mass changes. The method of Trépanier et al. (2016) could be applied in the studied area because all rocks are interpreted to be igneous and because analyses for Al_2O_3, TiO_2, Zr, and Y are available. The modelled precursors are presented by Table 3, and their major element concentrations are consistent with the rock types determined by Zr/Ti ratios (Fig. 3). Results of the modelling are presented as absolute mass changes (in grams) in Figure 4 and Table 4.

Altered andesite, dacite, and basalt display similar mass changes and altered rhyolite display the largest gains in SiO_2, MgO, and FeO_T (Fig. 4). Silica and Fe-Mg-metasomatism is particularly intense in rhyolite, with average gains of 15.27g SiO_2 and 4.72g FeO_T+MgO (for 100g of precursor). The alkali content was only modified in the rhyolite, which lost 3.34g of Na_2O+K_2O. The CaO content of rhyolites, on the other hand, was little modified, while andesite and basalt lost about 2.29g of CaO (Fig. 4, Table 4). In summary, most rocks gained Si and Fe-Mg, and lost Ca and/or Na-K.

Method 2: Field relations and petrography

Alteration, in the context of mineral assemblages, was established through field and petrographic observations. Complete mineralogical observations are not available for

Osisko's samples, on which normative calculations will be performed (see next section). In this section, the mineral content of samples collected in the field are reported and used to approximate the metamorphic grade, which is a pre-requirement for normative calculations.

Field and thin sections

The rocks observed in the field were named using their major constituent phases (Table 5). These rocks are medium- to coarse-grained, and their grain size and sulphide-content increase with proximity to the ore zone.

The calcic amphibole-bearing gneiss is the only unit with a mafic volcanic precursor. This unit is located in distal position relative to the massive-sulphide lenses, where it is in sharp contact with sillimanite-bearing schists. This gneiss contains mostly tremolite, green hornblende, plagioclase, and quartz (Table 5). The other units observed in the field are interpreted to have felsic volcanic precursors (i.e. rhyolite, possibly dacite).

Most units with felsic precursors have gradational contacts. Listed in order of increasing proximity to the deposit, these units are: 1) sillimanite-bearing schist; 2) sillimanite-cordierite-bearing schist; 3) cordierite-bearing schist; and 4) cordierite-anthophyllite-bearing gneiss. The anthophyllite-bearing gneiss may also have a felsic precursor, is proximal to the ore and forms patches or elongated curvi-linear spatially restricted domains.

The sillimanite-bearing schist displays compositional layering, with bands dominated by quartz and biotite with minor amounts of muscovite, microcline, and

plagioclase, and bands dominated by sillimanite, biotite, and quartz (Fig. 5a, b; Table 5). These minerals are part of the peak assemblage except for muscovite, which is late and likely retrograde. Other samples contain scattered sillimanite porphyroblasts instead of bands. The sillimanite-bearing and sillimanite-cordierite-bearing schists are similar in hand samples; however, only the latter contains cordierite, which is systematically porphyroblastic and poikiloblastic (Table 5).

The cordierite-bearing schist displays a light vitreous lustre typical of silicified rocks. The cordierite-anthophyllite-bearing gneiss is coarse grained, massive, light coloured, and may contain abundant pyrrhotite. Cordierite is porphyroblastic and poikiloblastic, and is hosted in a quartz-biotite-dominated groundmass (Fig. 5c, d; Table 5). The anthophyllite-bearing gneiss is dominated by quartz, plagioclase, anthophyllite, and biotite, and may contain pyrrhotite (Fig. 5e).

Muscovite is generally retrograde and is observed replacing sillimanite, biotite, and plagioclase. Chlorite is also retrograde, and replaces cordierite and biotite. Cordierite is often pinnitised (Fig. 5f).

In summary, for rocks with felsic precursors, distal units are dominated by quartz-biotite-sillimanite assemblages, while proximal ones contain mostly cordierite, quartz, biotite, and local anthophyllite. The abundance of Fe-Mg-Al-bearing phases, K-bearing phases (especially biotite), and quartz (Table 5) is likely the consequence of pre-metamorphic chloritisation, sericitisation, and silicification, respectively.

Metamorphic grade

The metamorphic grade is not well constrained at Coulon but needs to be roughly estimated prior to performing normative calculations (see next section). Mineralogical constraints were therefore used to select one of the models of CONSONORM_HG (Mathieu et al. 2016), which is a method that calculates simplified normative assemblages for various *P–T* conditions. The selected model calculates amphibolite facies minerals, including sillimanite, and corresponds to one of the following models: 6AMP600, 4AMP600, 7AMP700, 5AMP670, and 3AMP675 ("AMP" stands for amphibolite facies; the first and last numbers designate the pressure in kbar and the temperature in °C, respectively) (Fig. 6a).

Alteration of felsic rocks increased their Fe-Mg- and relative Al-contents, bringing their chemical composition closer to that of pelite. The well constrained petrogenetic grids for the KFMASH system (K_2O-FeO-MgO-Al_2O_3-SiO_2-H_2O) developed for pelites are used to interpret the assemblages of sillimanite and/or cordierite-bearing schists and then determine which CONSONORM_HG model is most appropriate. In the KMASH system, which is favoured here because the rocks observed in the field contain cordierite and lack garnet and staurolite (see AFM diagram; e.g. Spear 1995), only the 4AMP600, 5AMP670, and 3AMP675 models are within the stability field of cordierite (Spear and Cheney 1989; Fig. 6a). The 4AMP600 model is discarded because it is too close to the stability field of chlorite (Fig. 6a) which, although present at Coulon, is not part of the peak assemblage.

Microcline is observed in thin sections and is consistent with the 5AMP670 and 3AMP675 models, which are within or close to the stability field of K-feldspar (Fig. 6a). These models are also close to the H_2O-saturated solidus of the KFMASH system (Wei et

al. 2004), which is consistent with the migmatites that are reported at Coulon (Savard et al. 2013), even if leucosomes, assemblages characteristic of the vapor-absent melting of pelites (e.g. garnet-orthoclase or orthopyroxene-orthoclase; Spear 1995), and other anatexis evidences have not been identified in the field. Metamorphic conditions are likely close to the granitic liquidus at Coulon (i.e. upper amphibolite facies).

The rocks with felsic precursors observed in the field are K-poor chloritized rocks. Using a *P–T* pseudosection calculated for a K-poor metapelitic schist (Mezger and Régnier 2016; Fig. 6b), the 5AMP670 model is favoured because, contrarily to the 3AMP675 model, it is located outside of the stability field of muscovite, which is not part of the peak metamorphic assemblage of the cordierite-bearing rocks observed in the field.

Method 3: Normative minerals

In this section, normative calculations are performed with CONSONORM_HG, a method designed for mining exploration datasets (see Mathieu et al. 2016 for details), and alteration indices that correspond to ratios of normative minerals are proposed.

Normative calculations

Normative calculations using the CONSONORM_HG method, model 5AMP670, normative estimates of CO_2 and Fe_2O_3/Fe_2O_{3T} ratios of 0.2, 0.35, 0.4, and 0.5 for basalt, andesite, dacite, and rhyolite, respectively (following Middlemost 1989), are performed on the altered samples of the Osisko database (Tables 6, 7) and on the precursors (Table 3) predicted using the procedure of Trépanier et al. (2016) (Table 8) (see section “Method 1: mass balance calculations”).

To quantify chloritisation, for example, it is tempting to calculate chlorite proportions using a method designed for greenschist facies rocks, such as NORMAT (Piché and Jébrak 2004) or CONSONORM_LG (Trépanier et al. 2015). However, high-grade metamorphism likely modified the volatile (LOI) content of rocks and calculating low-grade normative assemblages with an erroneous LOI may result in under-estimation of the amount of pre-metamorphic carbonate and sulphide, and over-estimation of chlorite. Also, low-grade assemblages cannot be compared with minerals observed in the field. For these reasons, it was decided to calculate high-grade assemblages using the CONSONORM_HG method.

Results of this calculation are presented using 7 individual samples (Table 6). The samples that gained MgO and FeO_T, according to mass balance calculations, contain normative quartz, cordierite, and/or biotite. Similar assemblages characterise the cordierite-bearing rocks observed in the field. The silicified or chloritized samples that leached alkali (#3 and 4; Table 6) mostly contain quartz, sillimanite, alkali feldspar, biotite, and cordierite, which are assemblages similar to those of the sillimanite- and cordierite-bearing rocks observed in the field.

Results of the normative calculation, for the whole dataset, are summarised by circle diagrams (Figs. 7-10), which are complementary to the summary statistics provided in Tables 7 and 8. The circle diagrams have been designed to display normative mineral assemblages and to compare the altered rocks to their predicted precursors. The samples are plotted within circles with radius *R* and centers with Cartesian coordinates (*Cx, Cy*). To plot a sample in these diagrams, x and y coordinates are calculated using equation 1 and 2, in which factors are used to control the location of minerals (e.g. to locate

cordierite on the circle diagram in Figure 7, the factors used are $F_{cord} = Cx*\cos(\pi/3)+R$ and $G_{cord} = Cy*\sin(\pi/3)+R$).

$$x = (M_1*F_1 + M_2*F_2 + \ldots. + M_n*F_n) / (M_1 + M_2 + \ldots. + M_n) \quad \text{(equation 1)}$$

$$y = (M_1*G_1 + M_2*G_2 + \ldots. + M_n*G_n) / (M_1 + M_2 + \ldots. + M_n) \quad \text{(equation 2)}$$

where M_1, M_2, to M_n, are the proportions of the normative minerals displayed on the circle diagram; F_1, F_2, to F_n, and G_1, G_2, to G_n, are factors.

The first set of circle diagrams display the bulk of normative silicates (Fig. 7). Because assemblages can be difficult to read at first glance in such a diagram, additional diagrams dedicated to Fe-Mg-minerals (Fig. 8), Al-K-Na-minerals (Fig. 9), and Ca-minerals (Fig. 10) have been designed.

Using the first set of circle diagrams (Fig. 7), it is observed that precursors are mostly an assemblage of albite, orthoclase, quartz, and amphibole (Table 8, Fig. 7). Conversely, altered rocks contain more quartz, biotite, cordierite, white mica, amphibole, and/or talc. The circle diagrams of Figure 8 are used to confirm that altered rocks contain abundant normative cordierite, as well as biotite and Fe-Mg-enriched minerals such as talc, anthophyllite, and/or olivine. These minerals, especially cordierite, are relatively more abundant in altered rhyolite (Fig. 8a) than in other rock types (Fig. 8b, c, d), which suggests that these rocks were more intensely altered.

With respect to K-Na- and Al-bearing minerals, altered rocks tend to contain more biotite, and occasionally more muscovite and sillimanite, than their predicted precursors (Fig. 9). Increases in orthoclase or albite proportions are indicated for some samples (Fig.

9). The circle diagrams for Ca-bearing minerals show that the normative assemblages of altered rhyolite are similar to those of their precursors, indicating that Ca-metasomatism is minor to absent in these rocks (Fig. 10a). Minor variations are observed for basalt, andesite, and dacite, which contain either more tschermakite or less Ca-bearing minerals than their precursors (Fig. 10b, c, d).

Alteration indices

The normative differences observed between altered rocks and their precursors (see previous section) are used to propose alteration indices designed for the estimation of silicification, chloritisation, and sericitisation in high-grade metamorphic rocks. The numerator to these alteration indices correspond to a sum of minerals that are abundant in altered rocks (Table 7), while being generally absent in the calculated precursors (Table 8). The denominators are sums of silicates, with quartz generally excluded to ensure that the values of Index_FeMg and Index_K are independent of silicification.

To quantify silicification, only normative quartz can be used to calculate Index_Si (equation 3). Quartz, however, is not an ideal choice because all precursors contain quartz; i.e. the alteration index will not be equal to 0 for precursors.

$$\text{Index\_Si} = 100 * \text{quartz} / (\text{sum of all silicates}) \qquad \text{(equation 3)}$$

To quantify chloritisation, normative biotite, cordierite, anthophyllite, olivine, and talc (in wt%) are used to calculate Index_FeMg (equation 4). Normative olivine, talc, and

anthophyllite are used because even the most mafic precursors contain only minor amounts of these minerals (Table 8).

Index_FeMg = 100 * (cordierite + biotite + olivine + talc + anthophyllite) / (sum of all silicates - quartz) (equation 4)

To quantify sericitisation, normative muscovite and biotite are used to calculate Index_K (equation 5). To ensure that Index_K is equal to 0 for precursors, normative orthoclase, which is abundant in precursors (Table 8), is not used. However, sericitisation is an acidic alteration that induces the destruction of alkali feldspar and which may be more efficiently quantified by indices calculated using normative albite and orthoclase (i.e. Index_K-2 and Index_Na; equations 6 and 7).

Index_K = 100 * (muscovite + biotite) / (sum of all silicates - quartz) (equation 5)

Index_K-2 = 100 * (muscovite + biotite + orthoclase) / (sum of all silicates - quartz) (equation 6)

Index_Na = 100 * (albite + paragonite) / (sum of all silicates - quartz) (equation 7)

These indices have been calculated on all the available samples and on their precursors (Tables 7 and 8) to confirm that the values of the indices are the most elevated in altered rocks as should be expected. Index_FeMg indicates that chloritisation is most intense in the most felsic rocks. By subtracting the values that Index_Si takes in altered rocks and in their precursors, it can be concluded that silicification is most intense in

rhyolites. The values of Index_K indicate that altered rocks contain more micas than their precursors (Tables 7 and 8). The values of Index_K-2 and Index_Na indicate that the proportion of alkali-bearing phases has not been significantly modified by alteration, except for the altered rhyolite and dacite that contain less albite than their precursors.

The indices have also been calculated using the proportions of minerals observed in thin sections (Table 5). The values of Index_Si are most elevated in the sillimanite- and cordierite-bearing schists. Index_FeMg is progressively more elevated from sillimanite-bearing schist to cordierite-bearing and cordierite-anthophyllite-bearing gneiss, and is also elevated for the anthophyllite-bearing gneiss. Possibly, these rock types belong to the same felsic unit that becomes progressively chloritised closer to the mineralisation. The values for Index_K and Index_K-2 are inversely correlated to the values for Index_FeMg in the felsic unit. Values for Index_K calculated from observed assemblages (Table 5) are significantly greater than values calculated from normative assemblages (Table 7). This suggests discrepancies between observed and calculated assemblages (see discussion section). The calcic amphibole-bearing gneisses have lower indices values (Table 5) similar to those calculated for andesite and basalt (Table 7), and may correspond to slightly altered rocks with mafic to intermediate precursors.

Discussion

In this contribution, mass balance calculations and alteration indices, calculated using normative and observed minerals, are used to estimate the intensity of VMS-related alteration associated with the metamorphosed Coulon deposit. Each method provides

unique results, which are discussed and compared. The applicability of these methods in an exploration context and their sensitivity to metamorphic processes are then discussed.

Mass balance vs. normative calculations

Absolute mass changes, as presented here, provide estimates on the absolute loss and gain of major elements during alteration. Mass gains are generally independent of the composition of the precursor, while the amount of mass lost may be dependent on the precursor; i.e. a calcium-poor rock, for example, has little calcium to lose to alteration. Alteration indices, on the other hand, best approximate the amount of particular mineral phases gained during alteration and are generally not designed to reflect those lost to alteration.

Silicification induces SiO_2 mass gain and increase of normative quartz proportions. Quartz is used to calculate Index_Si but this mineral may not be an ideal choice because it may be consumed by metamorphic reactions (e.g. Fig. 6). Despite this problem, Index_Si correlates with SiO_2 mass changes (Fig. 11) and can be used to quantify silicification. Comparing Index_Si to SiO_2 mass changes (Fig. 11), it is also observed that rhyolite was subjected to more intense silicification than the other rock types (Fig. 11). Silicification results in SiO_2 mass gain > 0 and Index_SiO_2 > 42.04 (see precursors; Table 8), but is likely significant for SiO_2 mass gain > 10-20 g (Fig. 4) and Index_Si values > 60-70 (Fig. 11; Tables 7, 8).

Chloritisation induces FeO_T+MgO mass gains that, at Coulon, correspond to an increase of the normative proportions of cordierite, biotite, and/or Fe-Mg-phases (anthophyllite, etc.). The values of Index_FeMg correlate well with FeO_T+MgO mass

changes (Fig. 12), except for the least-altered mafic samples (Fig. 12b), and both methods indicate that chloritisation is most intense in rhyolite. Chloritisation initiates for both mass gains and index values > 0-1 but is likely significant for FeO_T+MgO mass gain > 2-5 g (Fig. 4) and Index_FeMg > 30-50 (Fig. 12; Tables 7, 8). Intense chloritisation is reflected by quartz-cordierite-biotite-anthophyllite normative assemblages and Index_FeMg values > 70-80.

Reconciling Index_K with K_2O mass changes is more challenging, as correlation is observed mostly for samples that lost K_2O (Fig. 13a). Improved correlations are displayed by Index_K-2 and K_2O mass changes (Fig. 13b), and correlations are also observed between Index_Na and Na_2O mass changes (Fig. 13c).

In rhyolite, sericitisation has induced alkali gains, which are likely significant for K_2O and/or Na_2O mass gains of > 1-2 g that correlate with indices values over about 50-60 (Fig. 13). More frequently, alkali losses are observed in rhyolite, which are characterised by K_2O and/or Na_2O mass loss > 1-2 g and Index_K-2 and/or Index_Na values < 20-40 (Fig. 13; Tables 7, 8). Alkali losses are either a consequence of sericitisation (alkali feldspar replaced by white mica, with or without K-gains) or chloritisation (white mica replaced by chlorite; e.g. Stanley and Madeisky 1994).

Alkali metasomatism is not significant in andesite and basalt, which mostly lost > 1-2 g of CaO (Fig. 4). In dacite, minor alkali and CaO losses are observed (Fig. 4). Feldspars have been destabilised in these rocks, likely as a consequence of sericitisation and/or chloritisation.

Normative vs. observed minerals

In the field, samples were collected from units with mafic (calcic amphibolite-bearing gneiss) and felsic (other rocks) precursors. The samples with felsic precursors are compared to the altered rhyolite of the Osisko dataset.

Minerals observed in thin sections, and related Index_Si, point to moderate Si-metasomatism for the anthophyllite-free samples with felsic precursors, for which 42.04 < Index_Si < 60-70 (Table 5). Index_FeMg for rocks with felsic precursors suggests moderate (distal sillimanite-bearing schist) to intense chloritisation (cordierite- and cordierite-anthophyllite-bearing gneisses) (Table 5).

Using Index_K-2, it could be concluded that most rocks leached moderate (sillimanite-cordierite-bearing schist) to large amount (cordierite- and cordierite-anthophyllite-bearing gneisses) of K_2O (see Index_K-2 < 20-40 for felsic units) (Table 5). However, this interpretation should be modified in light of the discrepancies between calculated and observed minerals that arise because, in the 5AMP670 model (CONSONORM_HG method), the compositional range for which the sillimanite-biotite-K-feldspar assemblage (see central part of the AFM diagram; e.g. Spear 1995) can be calculated is too small. Consequently, calculated assemblages are dominated by cordierite-biotite while, in the field, both cordierite-biotite and sillimanite-biotite assemblages are abundant. These discrepancies do not impair interpretation of Index_FeMg, which is calculated with both biotite and cordierite proportions. However in the field, alkali-leaching, which is a proxy to sericitisation, should be interpreted using sillimanite proportions for rocks with intermediate Fe/Mg ratios (i.e. cordierite-free rocks, such as the sillimanite-bearing schists), and using Index_K-2 for rocks with low Fe/Mg ratios (i.e. cordierite-bearing rocks).

Sensitivity of methods to metamorphism

Metamorphism is not an iso-chemical process but the amount of metasomatism experienced during metamorphism is minor in comparison to this induced by hydrothermal processes. Chemical methods such as mass balance and normative calculations are thus theoretically reliable in metamorphosed contexts. Carbonatation is minor to negligible at Coulon, where carbonate losses and calc-silicates phases gains (de-carbonatation) should not impair interpretations made from observed and normative minerals.

Massive sulphide lenses may have de-sulfurized and subsequent circulation of sulphur-bearing fluids may have induced Fe loss and decrease of the Fe/Mg ratios of silicates (Tomkins 2007). Identifying and quantifying this process at Coulon is beyond the scope of this paper and only its potential impact on the quantification of alteration is discussed. Index_FeMg is not sensitive to variations of Fe/Mg ratios. Mass balance and normative calculations may underestimate chloritisation intensity only if the circulation of sulphur-bearing fluids displaced significant amount of iron.

Anatexis is another process that is at play at Coulon. This process strongly modifies the chemistry of rocks, especially if leucosomes migrated, and may lead to erroneous quantification of hydrothermal alteration. Migmatites are locally abundant at Coulon, except in the “Main Area” (Savard et al. 2013) that was investigated in the field. Thus, it is only because anatexis is absent to minor in the study area that mass balance and normative calculations can be performed.

Quantifying alteration at Coulon

The main alteration types identified at Coulon are silicification, chloritisation, and sericitisation. In this section, after summarising the characteristics of these alteration types, the advantages and limits of the chemical methods used to quantify alteration are discussed.

The main chemical changes induced by alteration processes at Coulon are, according to mass balance calculations: 1) Si-gain (silicification); 2) Fe- and Mg-gain (chloritisation); and 3) alkali- (felsic precursors) and/or Ca- (mafic precursors) leaching (feldspar destruction likely induced by sericitisation) (Fig. 4). The method selected to perform these calculations (Trépanier et al. 2016) models the composition of precursors to provide precise quantification of mass changes that are easy to interpret. The main limitation of the method is that it applies to rocks with igneous precursors for which major elements and at least the trace element Zr have been analysed. These conditions are fulfilled at Coulon.

Alteration can also be characterised using normative assemblages. Silicification correlates with increasing proportions of normative quartz and is characterised by Index_Si values over about 40 to 60 for rocks with mafic to felsic precursors, respectively (Fig. 11). Chloritisation is best characterised by the normative assemblage cordierite+biotite±anthophyllite and Index_FeMg values > 30-50 (Fig. 12). At Coulon, sericitisation corresponds to feldspar destruction, possibly K-gains, and white mica formation. These white micas may then have been replaced by chlorite (chloritisation). The destruction of feldspar induced by sericitisation is best approximated with Index_K-2

and/or Index_Na values < 20-40, which mostly correspond to low normative proportions of orthoclase and albite.

Alteration indices can be calculated for most datasets (only the analysis of major elements is required), are reliable (see correlations with mass balance calculations), do not necessitate discrimination between rocks with igneous and sedimentary precursors, and can be easily correlated with observations made in the core shack (see next section). To interpret the value of some indices however (e.g. Index_Si), it is important to distinguish rocks with felsic and mafic precursors.

Estimating alteration at Coulon

In this section, recommendations are made to estimate alteration from observed minerals at Coulon. Observations made from hand samples enable the characterisation of large volumes of rocks; i.e. of the whole drill core instead of only the portions that have been chemically analysed.

Silicification is characterised by quartz proportions and, in hand samples, by a vitreous lustre. Comparing Index_Si to normative and observed quartz proportions (Tables 5 and 7) indicates that silicification is significant for quartz proportions over about 50 vol%. Sericitisation is not easily identified as white mica may have been, in part, replaced by chlorite during alteration, and as the remaining muscovite likely reacted with other minerals to form biotite during metamorphism (see Index_FeMg). Rocks with felsic precursors and dominated by sericitisation are characterised by quartz-biotite-sillimanite assemblages and contain minor amount of orthoclase and muscovite (sillimanite-bearing schists). In the field, sericitisation can be approximated using

sillimanite (distal felsic unit) and K-phases (see low values of Index_K-2 for proximal units that gained Fe-Mg).

Chloritisation, in felsic units, is characterised by cordierite, biotite and, in the most intensely altered rocks, anthophyllite. Chloritisation is correlated with relative decrease of Al_2O_3 (see decrease of sillimanite proportions). Based on comparison between Index_FeMg and the proportion of biotite and cordierite observed in thin sections, the following directives are proposed for estimating chloritisation of felsic units in the core shack: 1) rocks moderately chloritized are characterised by biotite+cordierite < 20-30 vol% and biotite > cordierite (e.g. sillimanite-cordierite-bearing schists); and 2) rocks intensely chloritized are characterised by biotite+cordierite of about 50 vol% and biotite < cordierite (e.g. cordierite- and cordierite-anthophyllite-bearing gneisses).

Alteration can be roughly estimated, in the core shack, using the proportions of observed quartz, sillimanite, K-phases (muscovite mostly, because feldspar can be difficult to identify), and dark-coloured phases (biotite and cordierite mostly).

Conclusions

The chemistry and mineralogy of the alteration halo of Coulon, a VMS-type deposit, have been investigated using mass balance calculations and alteration indices. Mass changes were calculated using modelled precursor compositions (method by Trépanier et al. 2016), a method valid at Coulon because precursors are igneous rocks, trace elements are analysed, and anatexis did not modify the chemistry of rocks. Alteration indices are calculated using normative (CONSONORM_HG method; Mathieu et al. 2016) and observed minerals. Indices calculated with normative minerals correlate

with mass changes. Comparing observed and normative minerals and their respective alteration indices indicate that rapid field (core shack) estimate of the main alteration types, for rocks with felsic precursors, can be made as follow: 1) silicification if quartz > 50 vol%; 2) moderate chloritisation if biotite+cordierite < 20-30 vol% and biotite > cordierite; and 3) intense chloritisation if biotite+cordierite ≥ 50 vol% and biotite < cordierite. Sericitisation is difficult to evaluate, but the intensity of alkali-leaching can be estimated from sillimanite and K-phases proportions. Coupling chemical and mineralogical methods enable precise punctual quantification (chemical analyses) and continuous estimate (field observations) of alteration at Coulon.

Acknowledgments

Special thanks are addressed to the geologists of Osisko Ltd. for contributing their data to this project. Also, we wish to address warm thanks to the associate editor T. Barresi, L. Corriveau, A. Bonnet, and to anonymous reviewers who greatly help us improve this contribution. This study was performed on behalf of the Consorem research group, which is supported by Canada Economic Development, the ministère de l'énergie et des ressources naturelles (MERN) du Québec, the conférence régionale des élus du Saguenay-Lac-Saint-Jean (CRÉ) and company members of Consorem. The Master thesis of Rose-Anne Bouchard is performed at the CERM, UQAC University, in collaboration with Osisko Ltd. and under the supervision of R. Daigneault. Warm thanks are also addressed to Sylvain Trépanier, Stéphane Faure, Ludovic Bigot, and Silvain Rafini for constructive discussions on this project.

References

Barth, T.F.W. 1959. Principles of classification and norm calculations of metamorphic rocks. The Journal of Geology, **67**: 135–152.

Barrett, T.J., and MacLean, W.H. 1994. Chemostratigraphy and hydrothermal alteration in exploration for VHMS deposits in greenstones and younger volcanic rocks. *In* Alteration and alteration processes associated with ore-forming systems. *Edited by* D.R. Lentz. Geological Association of Canada, Short Course Notes 11, pp. 433-467.

Bernier, L.R., and MacLean, W.H. 1993. Lithogeochemistry of a metamorphosed VMS alteration zone at Montauban, Grenville Province, Quebec. Exploration and Mining Geology, **2**(4): 367-386.

Bonnet, A L., Corriveau, L., and La Flèche, M.R. 2005. Chemical imprint of highly metamorphosed volcanic-hosted hydrothermal alterations in the La Romaine Supracrustal Belt, eastern Grenville Province, Quebec. Canadian Journal of Earth Sciences, **42**(10): 1783-1814.

Bonnet, A.L., and Corriveau, L. 2007. Alteration vectors to metamorphosed hydrothermal systems in gneissic terranes. *In* Mineral deposits of Canada: a synthesis of major deposit-types, district metallogeny, the evolution of geological provinces, and exploration methods. *Edited by* W.D. Goodfellow. Geological Association of Canada, Mineral Deposits Division, Special Publication no. 5, 2007, pp. 1035-1049.

Corriveau, L., and Spry, P.G. 2014. Metamorphosed Hydrothermal Ore Deposits. *In* Treatise on Geochemistry Vol. 13. *Edited by* S.D. Scott. Elsevier, pp. 175-194.

David, J., Maurice, C., and Simard, M. 2009. Datations isotopiques effectuées dans le nord-est de la Province du Supérieur - travaux de 1998, 1999 et 2000 / Isotopic datation from the NE Superior Province – data from 1998, 1999, 2000. MERN report (Ministère Énergie et Ressources Naturelles, Québec government), Report DV 2008-05, p. 92.

Franklin, J.M.., Gibson, H.L., Galley, A.G., and Jonasson, I.R. 2005. Volcanogenic massive sulfide deposits. Economic Geology 100th Anniversary, **98**: 523-560.

Froese, E. 1998. Metamorphism of hydrothermally altered rocks. *In* Current Research 1998-E. *Edited by* Geological Survey of Canada, pp. 193–196.

Galley, A.G., Hannington, M.D., and Jonasson, I.R. 2007. Volcanogenic massive sulphide deposits. *In* Mineral resources of Canada: a synthesis of major deposit-types, district metallogeny, the evolution of geological provinces, and exploration methods. *Edited by* W.D. Goodfellow. Geological Association of Canada Mineral Deposits Division, Special publication 5, ISBN-13: 978-1-897095-24-9, pp. 141-162.

Gauthier, M. 2000. Styles et répartition des gîtes métallifères du territoire de la Baie-James (Québec). Chronique de la Recherche minière, **539**: 17-61.

GEOROC – Geochemistry of Rocks of the Oceans and Continents. 2016. Max-Planck-Institut fürChemie. (http://georoc.mpch-mainz.gwdg.de/georoc/Start.asp) (accessed 30.03.2016).

Gosselin, C., and Simard, M. 2001. Geology of the Lac Gayot area (NTS 23M). MERN report (Ministère Énergie et Ressources Naturelles, Québec government), Report RG 2000-03, p. 28.

Grant, J.A. 1986. The isocon diagram - A simple solution to Gresen's equation for metasomatic alteration. Economic Geology, **81**: 1976-1982. doi:10.2113/gsecongeo.81.8.1976.

Grant, J.A. 2005. Isocon analysis: a brief review of the method and applications. Physics and Chemistry of the Earth, Parts A/B/C, **30(**17): 997-1004. doi:10.1016/j.pce.2004.11.003.

Gresens, R.L. 1967. Composition-volume relationships in metasomatism. Chemical Geology, **2**: 291-306. doi:10.1016/0009-2541(67)90004-6.

Hannington, M.D., de Ronde, C.D.J., and Petersen, S. 2005. Sea-floor tectonics and submarine hydrothermal systems. *In* Economic Geology 100th Anniversary Volume. *Edited by* Society of Economic Geologists. Littelton, Colorado, USA, pp. 111-141.

Hastie, A.R., Kerr, A.C., Pearce, J.A., and Mitchell, S.F. 2007. Classification of altered volcanic island arc rocks using immobile trace elements: development of the Th–Co discrimination diagram. Journal of Petrology, **48**(12): 2341-2357.

Ishikawa, Y., Sawaguchi, T., Iwaya, S., and Horiuchi, M. 1976. Delineation of prospecting targets for Kuroko deposits based on modes of volcanism of underlying dacite and alteration halos. Mining Geology, **26**: 105-117.

Katz, M.B. 1988. Metallogeny of early Precambrian granulite facies terrains. Precambrian Research, **39**(1): 77-84. doi: 10.1016/0301-9268(88)90052-6.

Le Bas, M.J., Le Maitre, R.W., Streckeisen, A., and Zanettin, B. 1986. A chemical classification of volcanic rocks based on the total alkali-silica diagram. Journal of petrology, **27**(3): 745-750.

Leitch, C.H.B., and Day, S.J. 1990. Newgres: a turbo pascal program to solve a modified version of gresens' hydrothermal alteration equation. Computers & Geosciences, **16**(7): 925-932.

Leitch, C.H.B., and Lentz, D.R. 1994. The Gresens approach to mass balance constraints of alteration systems: methods, pitfalls, examples. *In* Alteration and alteration processes associated with ore-forming systems. *Edited by* D.R. Lentz. Geological Association of Canada, Short Course Notes 11, pp. 161-192.

Liaghat, S., and MacLean, H. 1995. Lithogeochemistry of altered rocks at the New Insco VMS deposit, Noranda, Quebec. Journal of geochemical exploration, **52**(3): 333-350. doi:10.1016/0375-6742(94)00069-N.

MacLean, W.H., and Barrett, T.J. 1993. Lithogeochemical techniques using immobile elements. Journal of Geochemical Exploration, **48**(2): 109-133. doi:10.1016/0375-6742(93)90002-4.

Mathieu, L., Trépanier, S., and Daigneault, R. 2016. CONSONORM_HG: a new method of norm calculation for mid- to high-grade metamorphic rocks. Journal of Metamorphic Geology. **34**(1):1-15. doi:10.1111/jmg.12168.

Mezger, J.E., and Régnier, J.L. 2016. Stable staurolite-cordierite assemblages in K-poor metapelitic schists in Aston and Hospitalet gneiss domes of the central Pyrenees (France, Andorra). Journal of Metamorphic Geology. **34**(2): 167-190. doi:10.1111/jmg.12177.

Middlemost, E.A. 1989. Iron oxidation ratios, norms and the classification of volcanic rocks. Chemical Geology, **77**(1): 19-26.

Nesbitt, H.W., and Young, G.M. 1984. Prediction of some weathering trends of plutonic and volcanic rocks based on thermodynamic and kinetic considerations. Geochimica et Cosmochimica Acta, **48**(7): 1523-1534.

Nesbitt, H.W., and Young, G.M. 1989. Formation and diagenesis of weathering profiles. The Journal of Geology, **97**(2): 129-147.

Pan, Y., and Fleet, M.E. 1995. Geochemistry and origin of cordierite-orthoamphibole gneiss and associated rocks at an Archaean volcanogenic massive sulphide camp: Manitouwadge, Ontario, Canada. Precambrian Research, **74**(1): 73-89. doi:10.1016/0301-9268(95)00010-3.

Peck, W.H., and Smith, M.S. 2005. Cordierite-gedrite rocks from the Central Metasedimentary Belt boundary thrust zone (Grenville Province, Ontario): Mesoproterozoic metavolcanic rocks with affinities to the Composite Arc Belt. Canadian Journal of Earth Sciences, **42**(10): 1815-1828.

Piché, M., and Jébrak, M. 2004. Normative minerals and alteration indices developed for mineral exploration. Journal of Geochemical Exploration, **82**(1): 59-77. doi:10.1016/j.gexplo.2003.10.001.

Prabhu, M.K., and Webber, G.R. 1984. Origin of quartzofeldspathic gneisses at Montauban-les-Mines, Quebec. Canadian Journal of Earth Sciences, **21**(3): 336-345. doi:10.1139/e84-035.

Riverin, G., and Hodgson, C.J. 1980. Wall-rock alteration at the Millenbach Cu-Zn mine, Noranda, Quebec. Economic Geology, **75**(3): 424-444. doi: 10.2113/gsecongeo.75.3.424

Sarbas, B. 2008. The GEOROC database as part of a growing geoinformatics net-work. *In* Geoinformatics 2008, Data to Knowledge, Proceedings. *Edited by* S.R. Brady and A.K. Sinha. U.S. Geological Survey Scientific Investigations Report 2008-5172, pp. 42–43.

Savard, M., Roy, I., and Pearson, V. 2013. Technical Report and Recommendations 2013 Exploration Program, Coulon Project, Québec. Technical report NI-43-101 by Virginia Inc., p. 73.

Shand, SJ. 1943. The Eruptive Rocks. Edited by John Wiley, New York (2nd edition), p. 444.

Simard, M., Labbe, J.Y., Maurice, C., Lacoste, P., Leclerc, A., and Boily, M. 2010. synthesis of the northeastern superior province. MERN report (Ministère Énergie et Ressources Naturelles, Québec government), Report MM 2010-01, p. 190.

Spear, F.S. 1995. Metamorphic phase equilibria and pressure-temperature-time paths. Washington, Mineralogical Society of America, p. 799.

Spear, F.S., and Cheney, J.T. 1989. A petrogenetic grid for pelitic schists in the system SiO2-Al2O3-FeO-MgO-K2O-H2O. Contributions to Mineralogy and Petrology, **101**(2): 149-164.

Stanley, C.R., and Madeisky, H.E. 1994. Lithogeochemical exploration for hydrothermal ore deposits using Pearce element ratio analysis. In Alteration and alteration processes associated with ore forming systems. Edited by D.R. Lentz. Geological Association of Canada, Short Course Notes 11, pp. 193-211.

Thériault, R., and Chevé, S. 2001. Géologie de la région du lac Hurault (SNRC 23L). MERN report (Ministère Énergie et Ressources Naturelles, Québec government), Report RG 2000-11, p. 49.

Tiwary, A., and Deb, M. 1997. Geochemistry of hydrothermal alteration at the Deri massive sulphide deposit, Sirohi district, Rajasthan, NW India. Journal of Geochemical Exploration, **59**(2): 99-121.

Tomkins, A.G. 2007. Three mechanisms of ore re-mobilisation during amphibolite facies metamorphism at the Montauban Zn–Pb–Au–Ag deposit. Mineralium Deposita, **42**(6): 627-637. doi:10.1007/s00126-007-0131-9.

Tracy, A., Puritch, E., and Yassa, A. 2009. Technical report and resource estimate on the Coulon property James Bay area middle north Québec. Technical report NI-43-101 for Virginia Inc. by P&E Mining Consultants Inc., p. 207.

Trépanier, S., Mathieu, M., Daigneault, R., and Faure, S. 2016. Precursors predicted by artificial neural networks for mass balance calculations: Quantifying hydrothermal alteration in volcanic rocks. Computers and Geosciences, **89**: 32-43. doi: 10.1016/j.cageo.2016.01.003.

Trépanier, S., Mathieu, L., and Daigneault, R. 2015. CONSONORM_LG: new normative minerals and alteration indexes for low-grade metamorphic rocks. Economic Geology, **110**(8): 2127-2138. doi: 10.2113/econgeo.110.8.2127.

Wei, C.J., Powell, R., and Clarke, G.L. 2004. Calculated phase equilibria for low-and medium-pressure metapelites in the KFMASH and KMnFMASH systems. Journal of Metamorphic Geology, **22**(5): 495-508. doi: 10.1111/j.1525-1314.2004.00530.x.

Winchester, J.A., and Floyd, P.A. 1977. Geochemical discrimination of different magma series and their differentiation products using immobile elements. Chemical geology, **20**: 325-343.Zheng, Y.C., Gu, L., Tang, X., Wu, C., Li, C., and Liu, S. 2011. Geology and geochemistry of highly metamorphosed footwall alteration zones in the Hongtoushan volcanogenic massive sulfide deposit, Liaoning Province, China. Resource geology, **61**(2): 113-139.

Table captions

Table 1: Averaged chemical analyses of the Osisko database

Table 2: Averaged chemical analyses of the GEOROC database

Table 3: Averaged chemical composition of the precursors modelled using Trépanier's method (Trépanier et al. 2016)

Table 4: Absolute mass changes calculated for 100g of precursor

Table 5: Approximated and averaged proportions (vol%) of minerals observed in thin sections

Table 6: Normative assemblages and absolute mass changes calculated for 7 chemical analyses of the Osisko database (altered rocks)

Table 7: Averaged normative assemblages (wt%) calculated from the chemical analyses of the Osisko database (altered rocks)

Table 8: Averaged normative assemblages (wt%) calculated from the precursors modelled using the procedure of Trépanier et al. (2016)

Figure captions

Fig. 1. Geological maps of the Coulon greenstone belt; (a) Simplified map of the Gayot complex area adapted from Gosselin and Simard (2001), with Subprovinces divisions from Simard et al. (2010); (b) Map of the VMS system of the Coulon greenstone belt established by Virginia Ltd. (now Osisko Ltd.) in 2008, and adapted from Tracy et al. (2009) and Savard et al. (2013). In the legend, "felsic intrusions (gneiss)" designates the Maurel and Tramont suites.

Fig. 2. Binary diagrams comparing averaged major (in wt%) and trace (in ppm) elements, calculated from the Osisko Ltd. and GEOROC datasets (Tables 1, 2), for the following rock types: (a) rhyolite; (b) dacite; (c) andesite; and (d) basalt.

Fig. 3. Precursors predicted using the method of Trépanier et al. (2016) and displayed on the TAS diagram (Le Bas et al. 1986).

Fig. 4. Box plot diagrams displaying the results of mass balance calculations for altered rhyolite, dacite, andesite, and basalt. Absolute mass changes are calculated for 100g of precursor.

Fig. 5. (a) Sillimanite-bearing schist observed in natural light (undulating bands of quartz and biotite enriched in fibrolitic sillimanite are in contact with quartz-biotite-dominated bands); (b) sketch of sillimanite-bearing schist observed in thin section; (c) cordierite-bearing schist observed in natural light, which contains mostly biotite, quartz, and poikiloblastic and porphyroblastic cordierite; (d) sketch of cordierite-bearing schist observed in thin section; (e) anthophyllite-bearing gneiss containing mostly quartz, plagioclase, anthophyllite, and biotite; (f) cordierite grain and its pinnite aureole observed

in polarised light (cordierite-bearing schist). The following abbreviations are used: Sil (sillimanite), Mc (microcline), Bt (biotite), Crd (cordierite), and Qtz (quartz).

Fig. 6. (a) Extract from the petrogenetic grid for pelites in the KFMASH system (Spear and Cheney 1989), displaying the models of the CONSONORM_HG method (gray circles). KFASH and KMASH reactions are in dashed gray and solid black lines, respectively; (b) Simplified extract from a *P–T* pseudosection, KFMASH system, calculated by Mezger and Régnier (2016) for a K-poor metapelitic schist (sample 00-29). The following abbreviations are used: MgChl (Mg-chlorite), MgCrd (Mg-cordierite), Phl (Mg-biotite), Bt (biotite), Sil (sillimanite), Ky (kyanite), And (andalusite), Qtz (quartz), Kfs (orthoclase), Ms (muscovite), St (staurolite), and Grt (garnet).

Fig. 7. Circle diagrams used to display the proportions of normative silicates for the following rock types: (a) rhyolite; (b) dacite; (c) andesite; and (d) basalt. The numbers locate the samples of Table 6.

Fig. 8. Circle diagrams used to display the proportions of normative Fe-, and/or Mg-bearing silicates for (a) rhyolite and (b) dacite; (c) andesite; and (d) basalt. The numbers locate the samples of Table 6.

Fig. 9. Circle diagrams used to display the proportions of normative Na-, K-, and/or Al-bearing silicates for (a) rhyolite and (b) dacite; (c) andesite; and (d) basalt. The numbers locate the samples of Table 6.

Fig. 10. Circle diagrams used to display the proportions of normative calcite and Ca-bearing silicates for (a) rhyolite and (b) dacite; (c) andesite; and (d) basalt. The numbers locate the samples of Table 6.

Fig. 11. Binary diagrams comparing Index_Si to SiO_2 mass changes, for altered (a) rhyolite and (b) dacite, andesite, and basalt.

Fig. 12. Binary diagrams comparing Index_FeMg to FeO_T+MgO mass changes, for altered (a) rhyolite and (b) dacite, andesite, and basalt.

Fig. 13. Binary diagrams comparing K_2O mass changes to Index_K (a) and Index_K-2 (b), and comparing Na_2O mass changes to Index_Na (c).

Tables

Table 1: Averaged chemical analyses of the Osisko database

	Altered rhyolite		Altered dacite		Altered andesite		Altered basalt	
	Mean	**St.d.**	**Mean**	**St.d.**	**Mean**	**St.d.**	**Mean**	**St.d.**
SiO_2 (wt%)	74.11	*7.57*	63.24	*4.39*	59.84	*3.20*	53.43	*2.67*
TiO_2	0.20	*0.09*	0.53	*0.11*	0.94	*0.16*	1.28	*0.28*
Al_2O_3	11.98	*1.86*	14.66	*1.24*	15.53	*1.08*	15.79	*1.00*
FeO_T	3.25	*2.68*	6.26	*2.46*	7.70	*1.24*	10.69	*1.28*
MgO	2.88	*3.69*	3.96	*2.32*	4.55	*2.02*	5.64	*1.88*
MnO	0.05	*0.05*	0.09	*0.06*	0.11	*0.03*	0.17	*0.04*
CaO	1.03	*1.54*	3.13	*1.34*	3.52	*1.70*	6.31	*2.28*
Na_2O	1.59	*1.16*	3.04	*0.91*	3.79	*1.13*	3.23	*0.92*
K_2O	2.56	*1.26*	2.49	*0.76*	1.57	*0.85*	0.90	*0.71*
P_2O_5	0.02	*0.02*	0.15	*0.06*	0.19	*0.07*	0.22	*0.07*
LOI	1.27	*1.64*	1.05	*0.82*	0.87	*0.78*	0.66	*0.68*
Cr (ppm)	43.41	*119.00*	171.52	*195.31*	57.75	*173.47*	84.90	*125.36*
Ba	395.25	*309.71*	557.43	*246.41*	376.26	*269.28*	233.33	*142.66*
Zr	251.31	*64.09*	154.15	*41.51*	171.74	*31.54*	136.58	*39.43*
Sr	41.69	*84.60*	277.90	*200.66*	179.21	*167.07*	172.48	*84.35*
Y	49.36	*19.11*	32.89	*14.20*	28.79	*8.47*	27.08	*9.11*

Table 2: Averaged chemical analyses of the GEOROC database

	Unaltered rhyolite		Unaltered dacite		Unaltered andesite		Unaltered basalt	
	Mean	**St.d.**	**Mean**	**St.d.**	**Mean**	**St.d.**	**Mean**	**St.d.**
SiO_2 (wt%)	74.43	*1.58*	67.08	*1.76*	59.71	*1.98*	53.25	*1.44*
TiO_2	0.24	*0.11*	0.58	*0.1*	0.99	*0.16*	1.27	*0.28*
Al_2O_3	10.27	*2.27*	13.88	*1.91*	15.12	*1.4*	15.32	*1*
FeO_T	2.09	*0.51*	4.36	*0.58*	6.69	*0.78*	9.65	*1.06*
MgO	0.32	*0.29*	1.72	*0.39*	3.21	*0.57*	5.37	*0.76*
CaO	0.94	*0.43*	3.76	*0.63*	6.17	*0.75*	8.72	*0.59*
Na_2O	4.22	*0.23*	3.94	*0.16*	3.69	*0.13*	3.03	*0.22*
K_2O	4.02	*0.5*	2.48	*0.31*	2.08	*0.24*	1.03	*0.22*

Table 3: Averaged chemical composition of the precursors modelled using Trépanier's method (Trépanier et al. 2016)

	Unaltered rhyolite		Unaltered dacite		Unaltered andesite		Unaltered basalt	
	Mean	**St.d.**	**Mean**	**St.d.**	**Mean**	**St.d.**	**Mean**	**St.d.**
SiO_2 (wt%)	74.02	*2.68*	63.4	*3.93*	59.17	*1.96*	54.09	*1.38*
TiO_2	0.23	*0.11*	0.57	*0.10*	0.95	*0.16*	1.27	*0.27*
Al_2O_3	13.38	*1.81*	15.8	*0.93*	17.13	*0.87*	16.88	*0.77*
FeO_T	2.07	*0.64*	4.86	*0.85*	6.77	*0.75*	9.51	*1.02*
MgO	1.08	*0.39*	3.55	*2.05*	3.91	*1.69*	5.28	*1.22*
CaO	1.43	*1.31*	6.03	*1.91*	6.51	*0.95*	8.70	*0.70*
Na_2O	3.98	*0.34*	3.52	*0.48*	3.62	*0.33*	3.12	*0.25*
K_2O	3.81	*0.33*	2.27	*0.62*	1.95	*0.36*	1.15	*0.26*

Table 4: Absolute mass changes calculated for 100g of precursor

Mass changes (g)	Rhyolite		Basalt + andesite + dacite	
	Mean	St.d.	Mean	St.d.
FeO_T	1.97	*5.23*	1.13	*1.69*
MgO	3.70	*7.29*	0.72	*3.20*
FeO_T + MgO	4.72	*10.01*	1.63	*4.62*
K_2O	-1.02	*1.42*	-0.20	*0.98*
Na_2O	-2.37	*1.37*	0.05	*1.13*
K_2O + Na_2O	-3.34	*2.09*	-0.15	*0.90*
SiO_2	15.27	*23.20*	-0.05	*6.07*
CaO	1.84	*79.06*	-2.29	*2.23*
n samples	**2555**		**2986**	

Table 5: Approximated and averaged proportions (vol%) of minerals observed in thin sections

Schists and gneiss	Sillimanite-bearing		Sillimanite-cordierite-bearing		Cordierite-bearing		Cordierite-anthophyllite-bearing		Anthophyllite-bearing		Calcic amphibole-bearing	
	Mean	**St.d.**	**Mean**	**St.d.**	**Mean**	**St.d.**	**Mean**	**St.d.**	**Mean**	**St.d.**	**Mean**	**St.d.**
Quartz	45	*15*	51	*10*	44	*16*	32	*14*	38	*31*	28	*10*
Biotite	20	*11*	17	*6*	24	*11*	11	*11*	10	*0.3*	9	*7*
Muscovite	7	*5*	2	*2*			2	*5*			5	*8*
Plagioclase	8	*7*	7	*3*	1	*1*	3	*4*	29	*19*	20	*10*
Microcline	5	*7*	2	*3*								
Cordierite			8	*6*	30	*7*	38	*19*				
Sillimanite	15	*9*	13	*6*								
Anthophyllite[(A)]							14	*11*	23	*12*		
Tremolite											11	*10*
Hornblende											27	*11*
Other[(b)]	<1		<1		<1		<1		<1		<1	
n sections	**11**		**3**		**7**		**10**		**2**		**5**	
Index_Si	44.9	*14.7*	51.4	*9.8*	44.5	*16.4*	32.1	*13.8*	37.7	*30.9*	28.3	*10.4*
Index_FeMg	37.1	*17.4*	52.9	*9.6*	98	*1.8*	92	*10.1*	56.2	*8.7*	13.7	*11.2*
Index_K	50.4	*17.7*	37.4	*9.3*	43.8	*9.5*	21.5	*17.5*	18.8	*9*	19.3	*12.6*
Index_K-2	58.4	*12.9*	41.1	*14.4*	43.8	*9.5*	21.5	*17.5*	18.8	*9*	19.3	*12.6*

[(A)]Anthophyllite or gedrite (the distinction could not be made)

[(B)]Other: chlorite, pinnite, zircon, opaque.

Table 6: Normative assemblages and absolute mass changes calculated for 7 chemical analyses of the Osisko database (altered rocks)

Precursor	**Rhyolite**	**Rhyolite**	**Rhyolite**	**Rhyolite**	**Dacite**	**Andesite**	**Basalt**
Main alteration	**Chloritisation (intense)**	**Chloritisation (moderate)**	**Chloritisation**	**Silicification**	**Chloritisation (moderate)**		
Elements leached	**alkali**	**alkali**	**alkali, Si**	**alkali**	**Ca**	**Ca**	**Ca, Na**
Nb (Figs. 7-10)	**1**	**2**	**3**	**4**	**5**	**6**	**7**
Normative minerals (wt%)							
Albite	0.87	1.00	0.16	8.99	34.68	40.38	0
Orthoclase	0	7.89	0	13.98	0	0	0
Anorthite	0	1.56	1.08	0	0	0	13.73
Muscovite	0	11.38	0.95	0	0	0	2.02
Paragonite	0	8.78	4.87	0	0	0	5.97
Biotite	12.64	10.79	24.55	0	9.32	14.53	42.92
Cordierite	31.4	0	25.03	0.08	20.22	17.78	11.39
Quartz	32.31	55.49	34.70	61.39	26.35	5.28	15.72
Sillimanite	0	0	0.20	12.54	0	0	0
Clinoamphibole	4.63	0	1.56	0	3.83	11.42	0
Olivine	0	0	0	0	0	0.37	0
Talc	12.84	0	0	0	1.77	3.69	0
FeTi-oxides	5.31	3.11	6.90	0.66	3.84	6.54	5.43
Carbonates	0	0	0	2.36	0	0	2.81
Mass changes (g) for 100g of precursor							
FeO_T	4.02	0.29	5.69	-1.21	1.36	0.52	0.36
MgO	12.67	2.74	8.77	0.11	4.32	3.21	4.04
K_2O	-2.42	1.27	-1.28	-0.94	-0.75	-0.38	2.71
Na_2O	-4.05	-3.4	-3.74	-3.04	0.36	1.42	-2.78
SiO_2	-4.11	22.2	-11.84	23.78	2.77	-7.22	-15.49
CaO	-0.47	-1.03	-0.81	-0.72	-3.42	-5.78	-3.41

Table 7: Averaged normative assemblages (wt%) calculated from the chemical analyses of the Osisko database (altered rocks)

	Altered rhyolite		Altered dacite		Altered andesite		Altered basalt	
	Mean	**St.d.**	**Mean**	**St.d.**	**Mean**	**St.d.**	**Mean**	**St.d.**
Albite	12.7	*10.67*	24.65	*8.43*	29.46	*9.55*	20.97	*9.49*
Orthoclase	11.31	*9.41*	9.00	*5.95*	3.49	*4.25*	2.97	*2.72*
Anorthite	1.95	*2.62*	8.49	*6.00*	6.80	*6.48*	3.05	*5.73*
Muscovite	2.79	*5.51*	0.20	*1.64*	0.12	*0.97*	0.02	*0.30*
Paragonite	1.07	*2.29*	0.16	*1.23*	0.12	*1.01*	0.04	*0.60*
Biotite	3.41	*5.34*	9.72	*6.87*	9.83	*8.15*	3.97	*7.84*
Cordierite	11.65	*8.02*	8.28	*7.00*	7.75	*7.32*	3.14	*6.71*
Garnet[(A)]	0.03	*0.39*	0	*0*	0.02	*0.57*	0.92	*4.74*
Quartz	46.93	*12.63*	25.67	*7.28*	20.54	*5.44*	14.05	*5.46*
Sillimanite	1.03	*1.83*	0.10	*0.48*	0.62	*1.25*	0.54	*1.57*
Anthophyllite	0.11	*2.02*	0.02	*0.20*	0.25	*1.57*	2.02	*2.92*
Clinoamphibole[(B)]	0.71	*5.16*	5.10	*11.15*	12.48	*13.94*	40.16	*18.5*
Clinopyroxene	0.01	*0.34*	0.03	*0.52*	0.01	*0.08*	0.21	*2.17*
Orthopyroxene	0	*0*	0	*0*	0.01	*0.37*	0.01	*0.27*
Olivine	0.02	*0.23*	0.12	*0.44*	0.11	*0.40*	0.87	*1.12*
Talc	1.09	*5.41*	1.18	*4.47*	0.54	*3.22*	0.05	*1.07*
Other silicate[(C)]	0.29	*2.39*	0	*0*	0.06	*0.82*	0.38	*1.99*
FeTi-oxides	3.10	*2.10*	5.53	*1.72*	6.57	*0.93*	5.69	*0.74*
Carbonates	1.44	*3.69*	1.13	*2.02*	0.57	*1.39*	0.24	*1.15*
Other[(D)]	0.38	*0.49*	0.61	*0.29*	0.65	*0.24*	0.71	*0.23*
n samples	**2597**		**295**		**779**		**1912**	
Index_Si	49.1	*12.84*	27.65	*7.81*	22.27	*5.89*	15.06	*5.88*
Index_FeMg	34.78	*24.50*	29.42	*15.21*	26.11	*18.22*	12.89	*17.34*
Index_K	15.25	*22.17*	15.22	*11.81*	14.22	*12.11*	5.32	*10.60*
Index_K-2	37.59	*16.88*	28.39	*8.76*	18.95	*10.98*	9.02	*9.60*
Index_Na	27.41	*17.29*	37.01	*11.50*	41.20	*12.42*	26.37	*11.44*

[(A)] Garnet = pyrope + almandine

[(B)] Clinoamphibole = pargasite + tschermakite + tremolite

[(C)] Other silicate = amesite + grossular + kalsilite + leucite + nepheline + spessartine + rhodonite

[(D)] Other = sulphide + sulphate + apatite + brucite + corundum + graphite

Table 8: Averaged normative assemblages (wt%) calculated from the precursors modelled using Trépanier's method (Trépanier et al. 2016)

	Unaltered rhyolite		**Unaltered dacite**		**Unaltered andesite**		**Unaltered basalt**	
	Mean	**St.d.**	**Mean**	**St.d.**	**Mean**	**St.d.**	**Mean**	**St.d.**
Albite	31.40	*6.03*	31.91	*2.04*	28.47	*2.34*	16.87	*3.40*
Orthoclase	20.00	*4.93*	14.66	*2.44*	12.52	*1.53*	6.88	*1.20*
Anorthite	1.09	*1.87*	8.96	*3.73*	15.10	*4.15*	12.81	*2.43*
Quartz	40.44	*8.47*	27.09	*3.00*	15.68	*4.66*	12.26	*2.85*
Biotite	0.06	*0.44*	0.45	*1.88*	0	*0*	0	*0*
Sillimanite	0.06	*0.37*	0	*0*	0	*0*	0	*0*
Anthophyllite	0	*0.03*	0	*0*	0	*0*	0.01	*0.06*
Cordierite	0.16	*0.70*	0.07	*0.35*	0	*0*	0	*0*
Clinoamphibole[(A)]	1.44	*1.35*	10.58	*5.07*	20.91	*3.83*	45.95	*5.24*
Olivine	0.01	*0.02*	0	*0*	0	*0*	0.01	*0.03*
Clinopyroxene	0.91	*1.23*	2.58	*4.60*	2.22	*4.63*	0.42	*2.67*
Talc	0.01	*0.25*	0	*0*	0	*0*	0	*0*
Other silicates [(B)]	0.94	*0.85*	0.04	*0.23*	0	*0*	0	*0*
FeTi-oxides	2.19	*0.60*	3.62	*0.52*	5.09	*0.64*	4.81	*0.66*
n samples	**2597**		**295**		**779**		**1912**	
Index_Si	42.04	9.67	28.12	3.17	16.52	4.88	12.86	2.92
Index_FeMg	0.40	2.32	0.77	3.12	0	0	0	0.12
Index_K	0.10	0.69	0.66	2.76	0	0	0	0
Index_K-2	35.49	6.90	21.78	3.08	15.85	2.19	8.31	1.54
Index_Na	55.89	6.08	46.17	3.58	35.97	2.83	20.32	3.96

[(A)] Clinoamphibole = pargasite + tschermakite + tremolite

[(B)] Other silicate = garnet + white micas + wollastonite

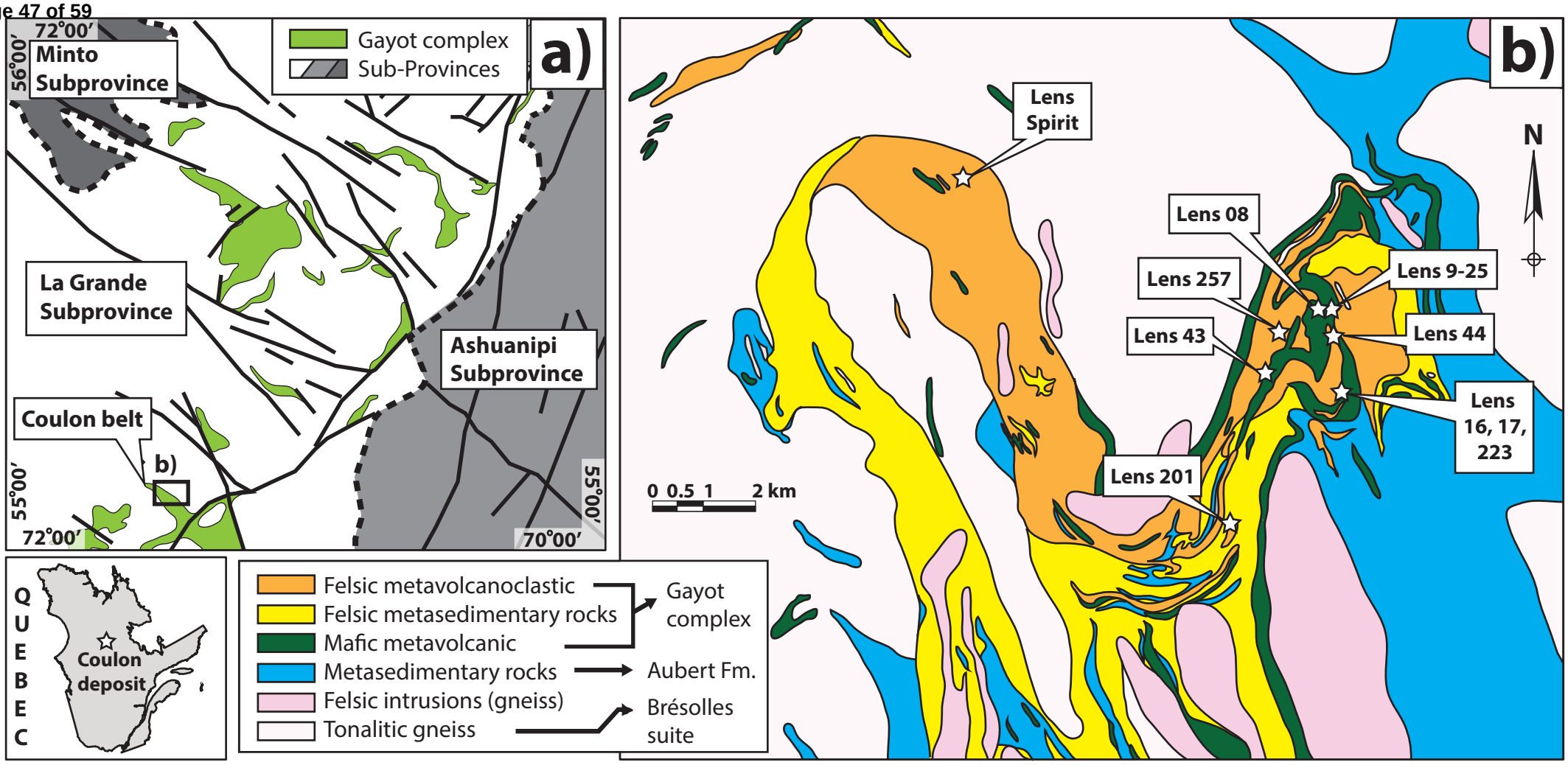
a)
Gayot complex
Sub-Provinces
72°00′
56°00′
Minto Subprovince
La Grande Subprovince
Ashuanipi Subprovince
Coulon belt
b)
55°00′
70°00′
QUEBEC
Coulon deposit
b)
Lens Spirit
Lens 08
Lens 257
Lens 43
Lens 9-25
Lens 44
Lens 16, 17, 223
Lens 201
N
0 0.5 1 2 km
Felsic metavolcanoclastic
Felsic metasedimentary rocks
Mafic metavolcanic
Metasedimentary rocks
Felsic intrusions (gneiss)
Tonalitic gneiss
Gayot complex
Aubert Fm.
Brésolles suite

Fig. 1

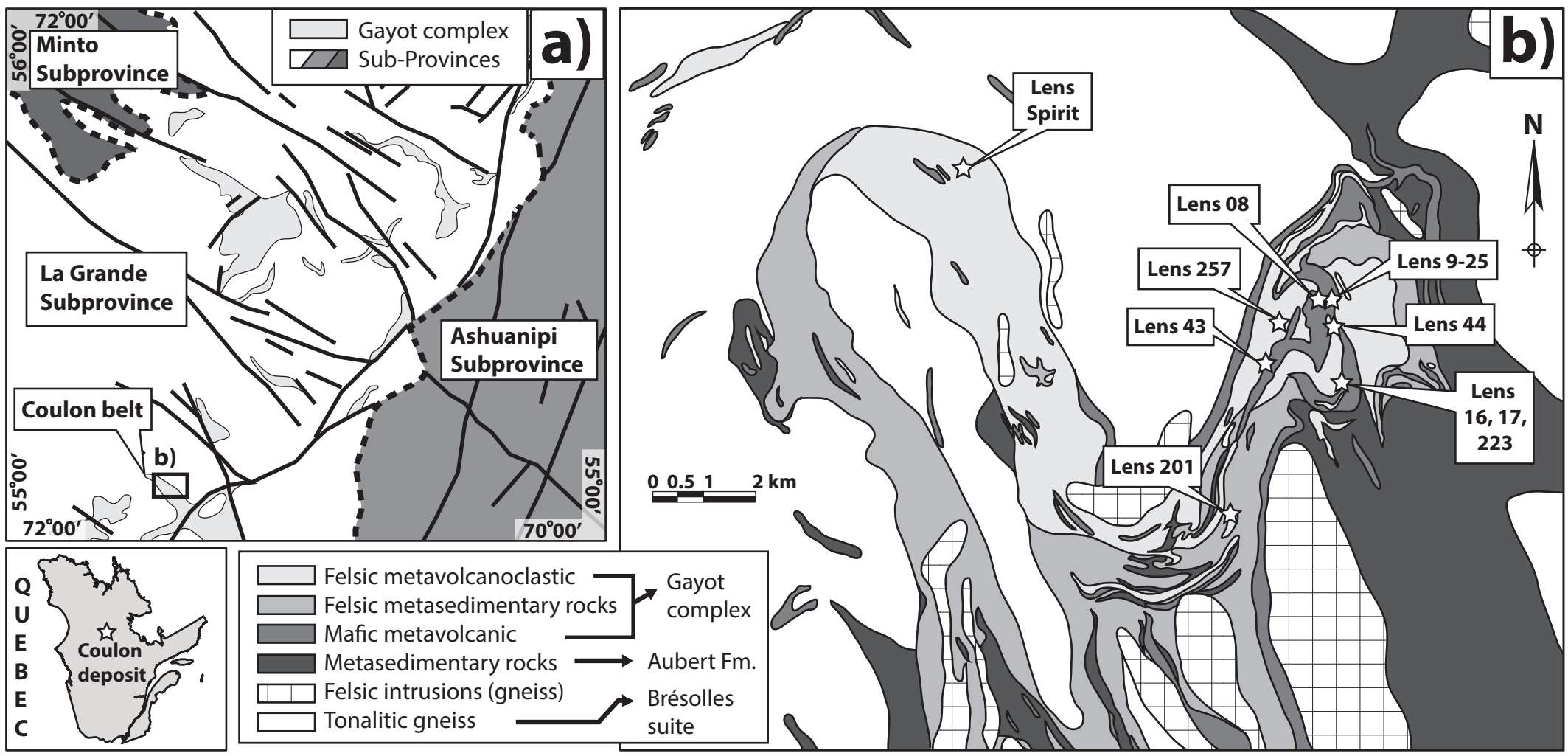
a)
Gayot complex
Sub-Provinces
72°00′
56°00′
Minto Subprovince
La Grande Subprovince
Ashuanipi Subprovince
Coulon belt
b)
55°00′
70°00′
QUEBEC
Coulon deposit
b)
Lens Spirit
Lens 08
Lens 257
Lens 43
Lens 9-25
Lens 44
Lens 16, 17, 223
Lens 201
N
0 0.5 1 2 km
Felsic metavolcanoclastic
Felsic metasedimentary rocks
Mafic metavolcanic
Metasedimentary rocks
Felsic intrusions (gneiss)
Tonalitic gneiss
Gayot complex
Aubert Fm.
Brésolles suite

Fig. 1

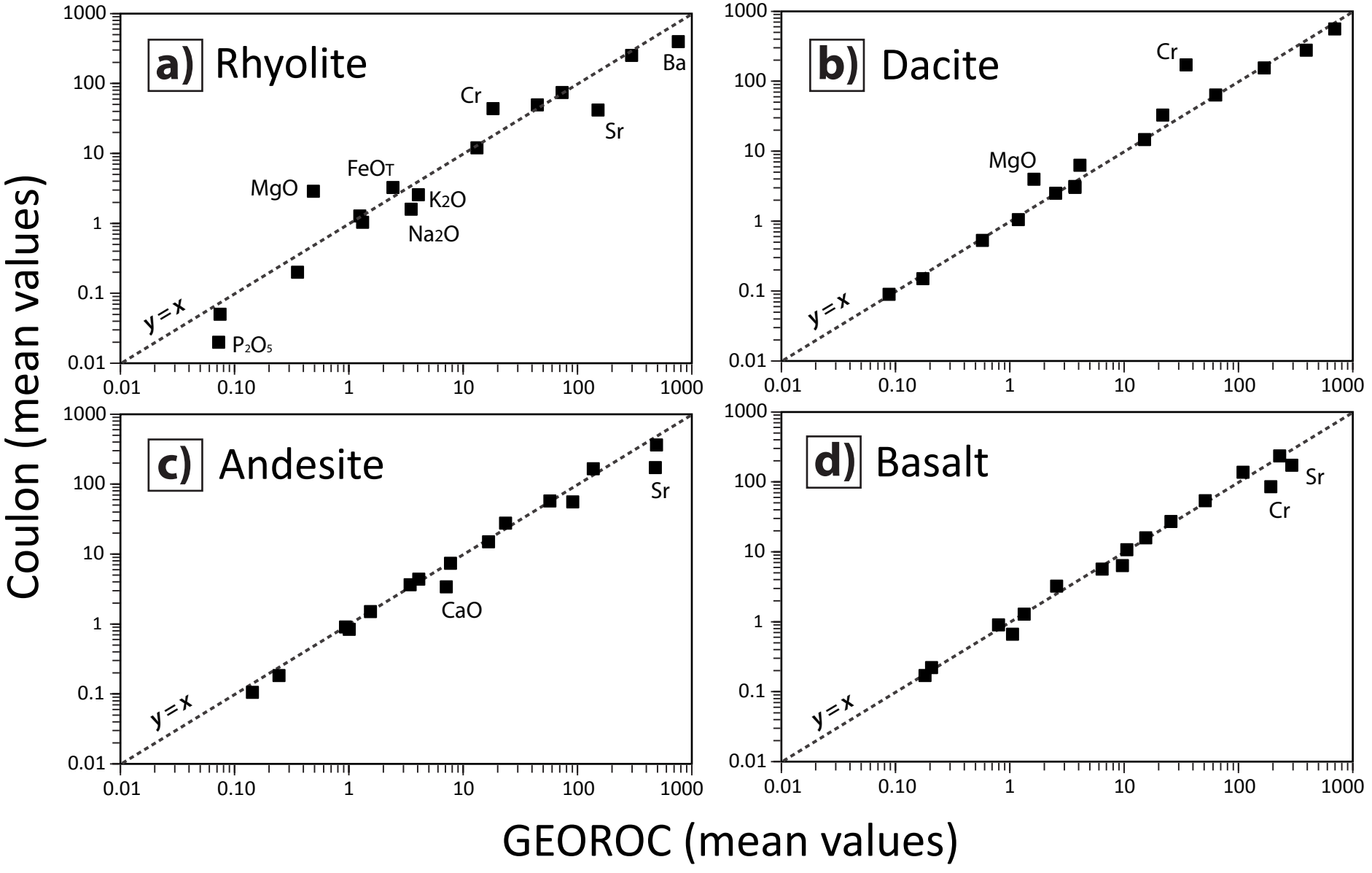
a) Rhyolite
b) Dacite
c) Andesite
d) Basalt
Coulon (mean values)
GEOROC (mean values)
y=x
MgO
FeOT
K2O
Na2O
P2O5
Cr
Sr
Ba
CaO
0.01
0.10
1
10
100
1000

Fig. 2

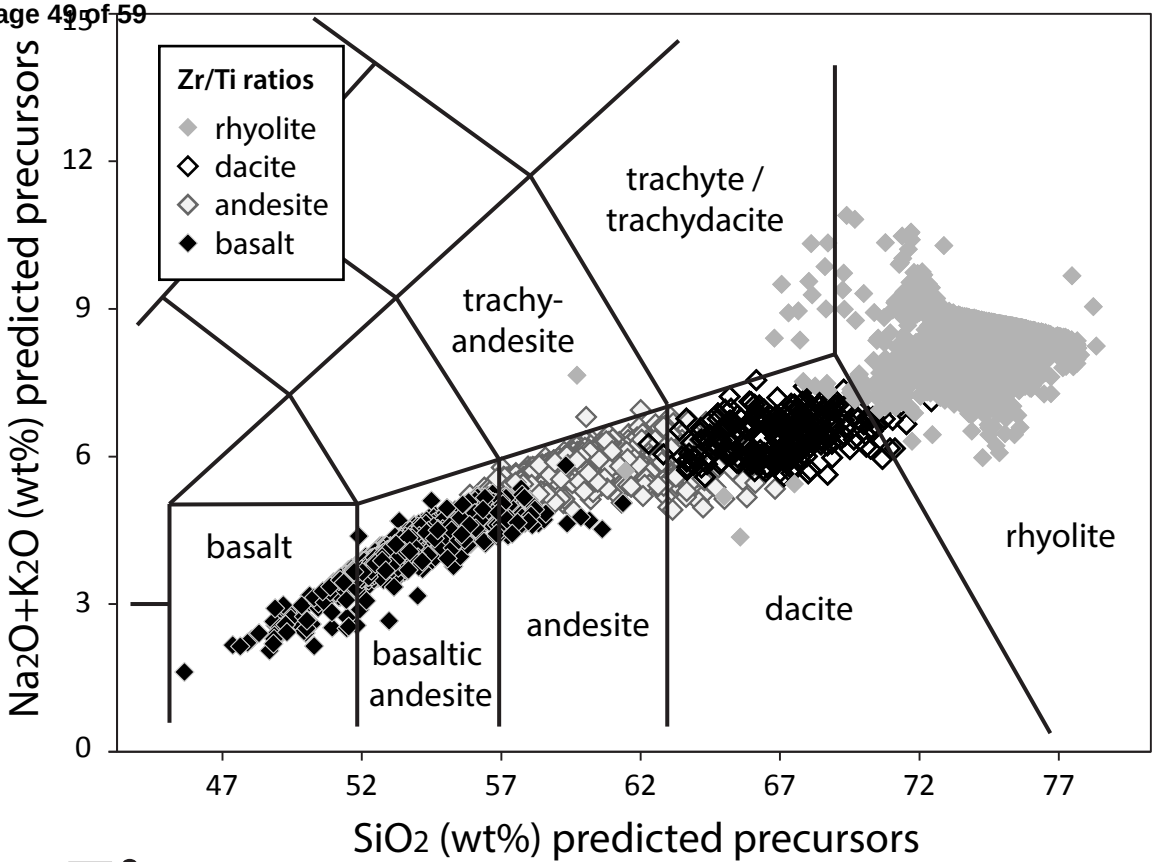
Zr/Ti ratios
rhyolite
dacite
andesite
basalt
trachyte / trachydacite
trachy-andesite
basalt
basaltic andesite
andesite
dacite
rhyolite
Na2O+K2O (wt%) predicted precursors
SiO2 (wt%) predicted precursors
0
3
6
9
12
15
47
52
57
62
67
72
77

Fig. 3

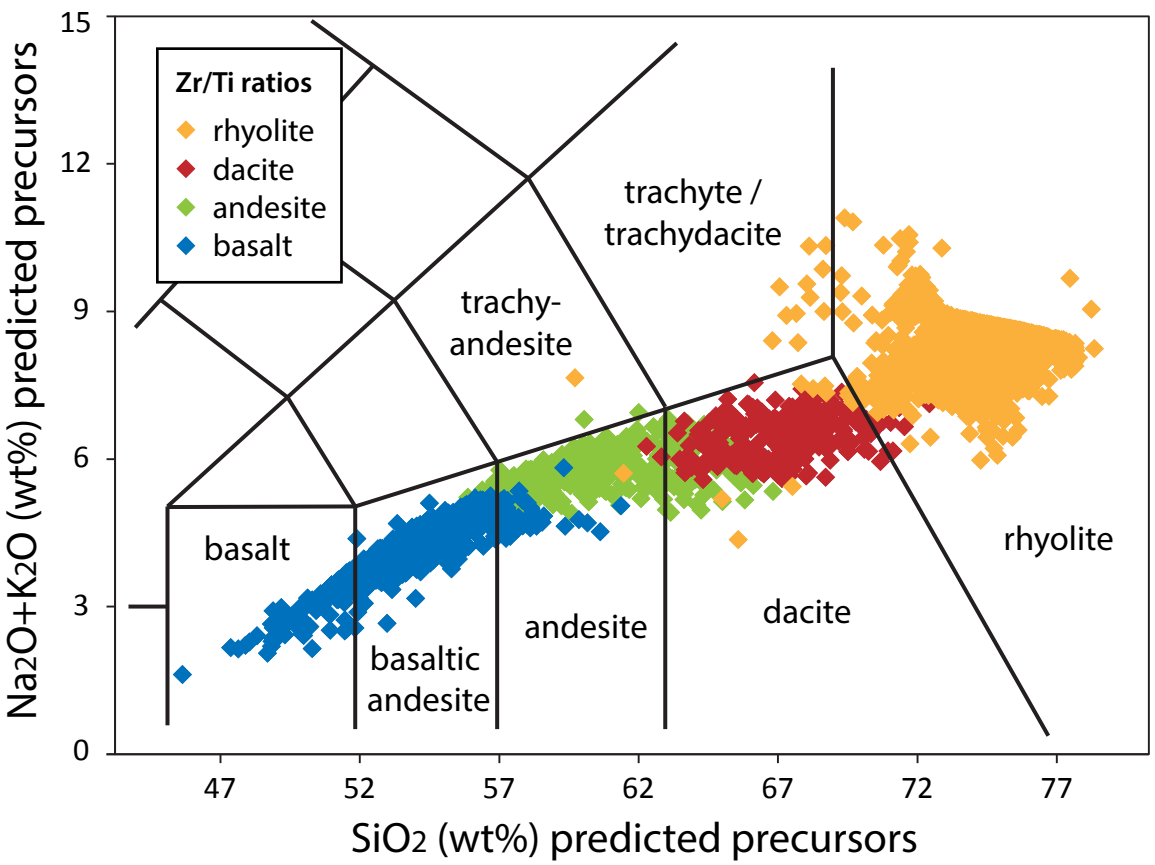
Zr/Ti ratios
rhyolite
dacite
andesite
basalt
trachyte / trachydacite
trachy-andesite
basalt
basaltic andesite
andesite
dacite
rhyolite
Na2O+K2O (wt%) predicted precursors
SiO2 (wt%) predicted precursors
0
3
6
9
12
15
47
52
57
62
67
72
77

Fig. 3

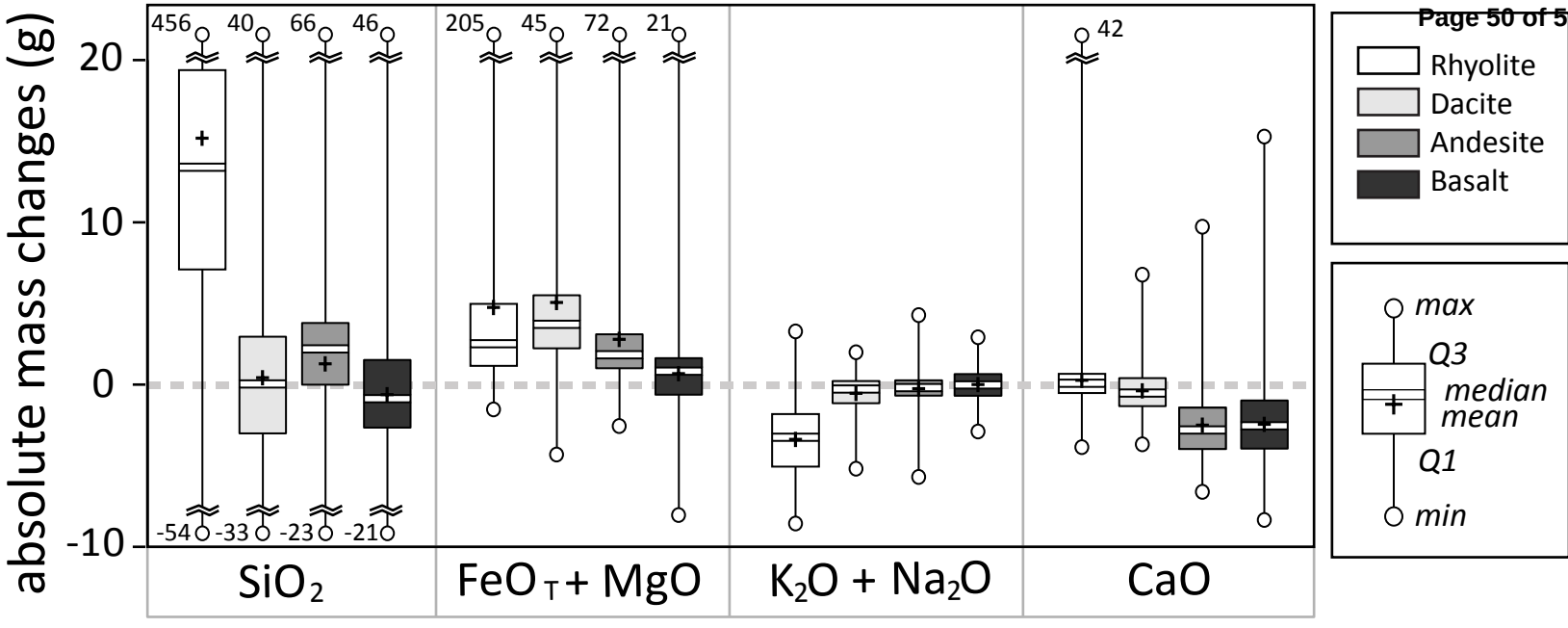
absolute mass changes (g)
20
10
0
-10
456
40
66
46
205
45
72
21
42
-54
-33
-23
-21
SiO2
FeOT + MgO
K2O + Na2O
CaO
Rhyolite
Dacite
Andesite
Basalt
max
Q3
median
mean
Q1
min

Fig. 4

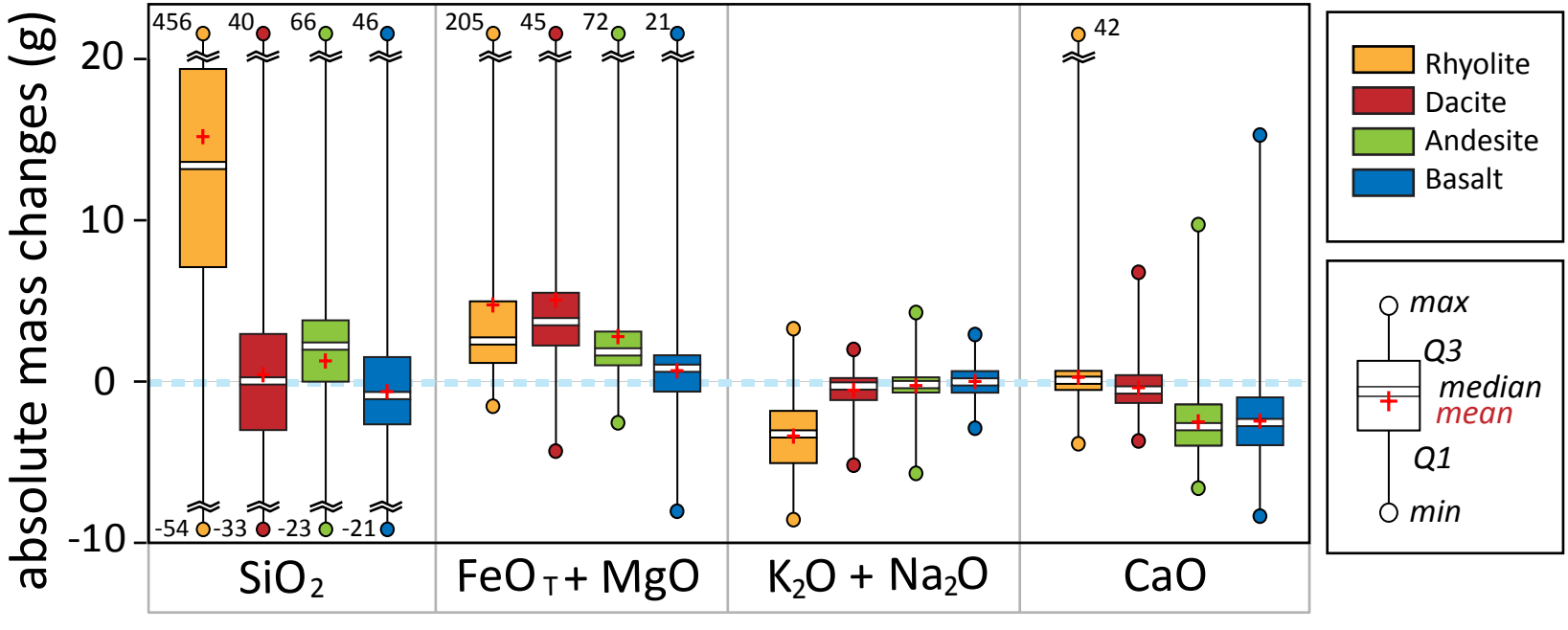
absolute mass changes (g)
20
10
0
-10
456
40
66
46
205
45
72
21
42
-54
-33
-23
-21
SiO2
FeOT + MgO
K2O + Na2O
CaO
Rhyolite
Dacite
Andesite
Basalt
max
Q3
median
mean
Q1
min

Fig. 4

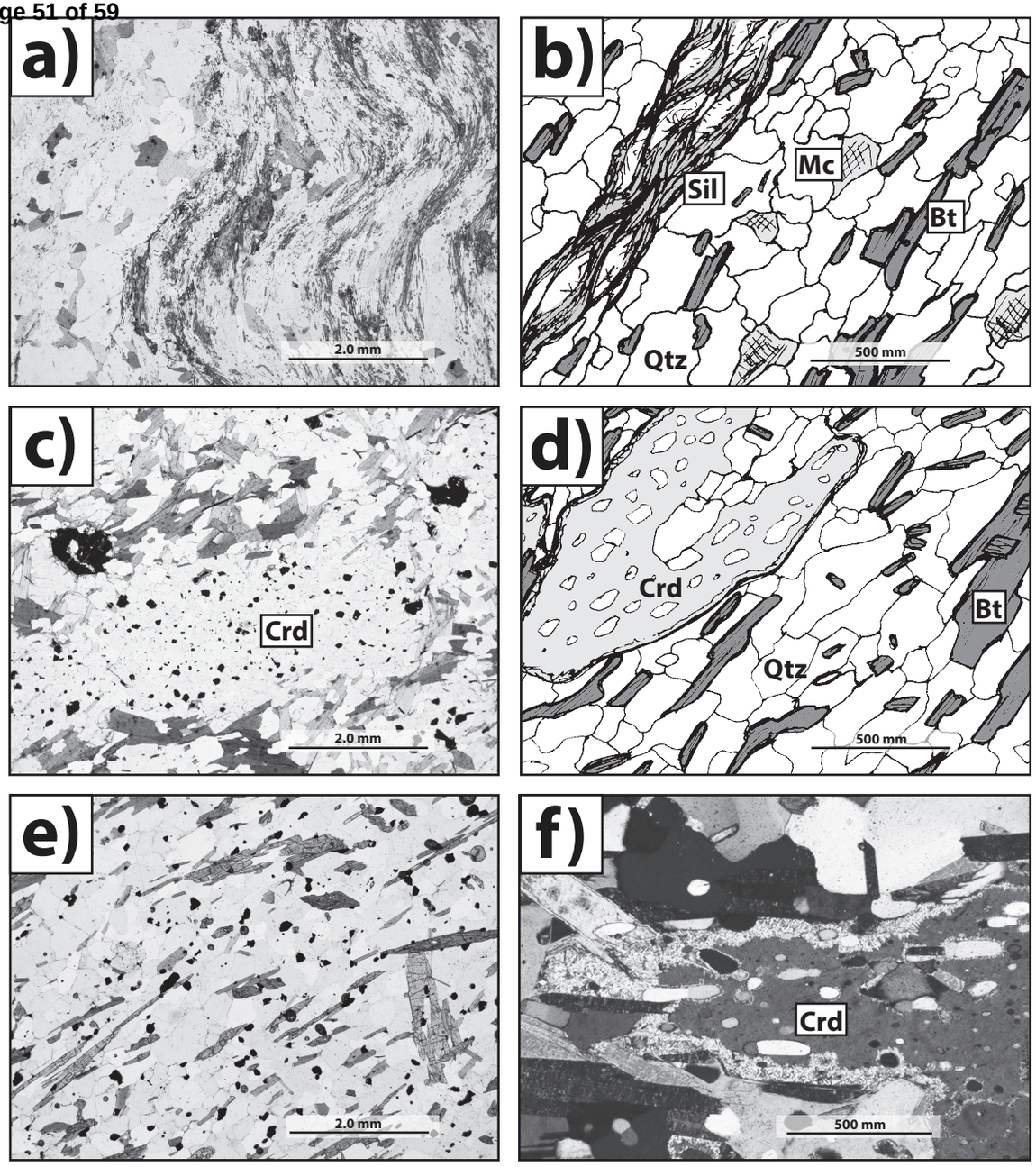
a)
2.0 mm
b)
Sil
Mc
Bt
Qtz
500 mm
c)
Crd
2.0 mm
d)
Crd
Bt
Qtz
500 mm
e)
2.0 mm
f)
Crd
500 mm

Fig. 5

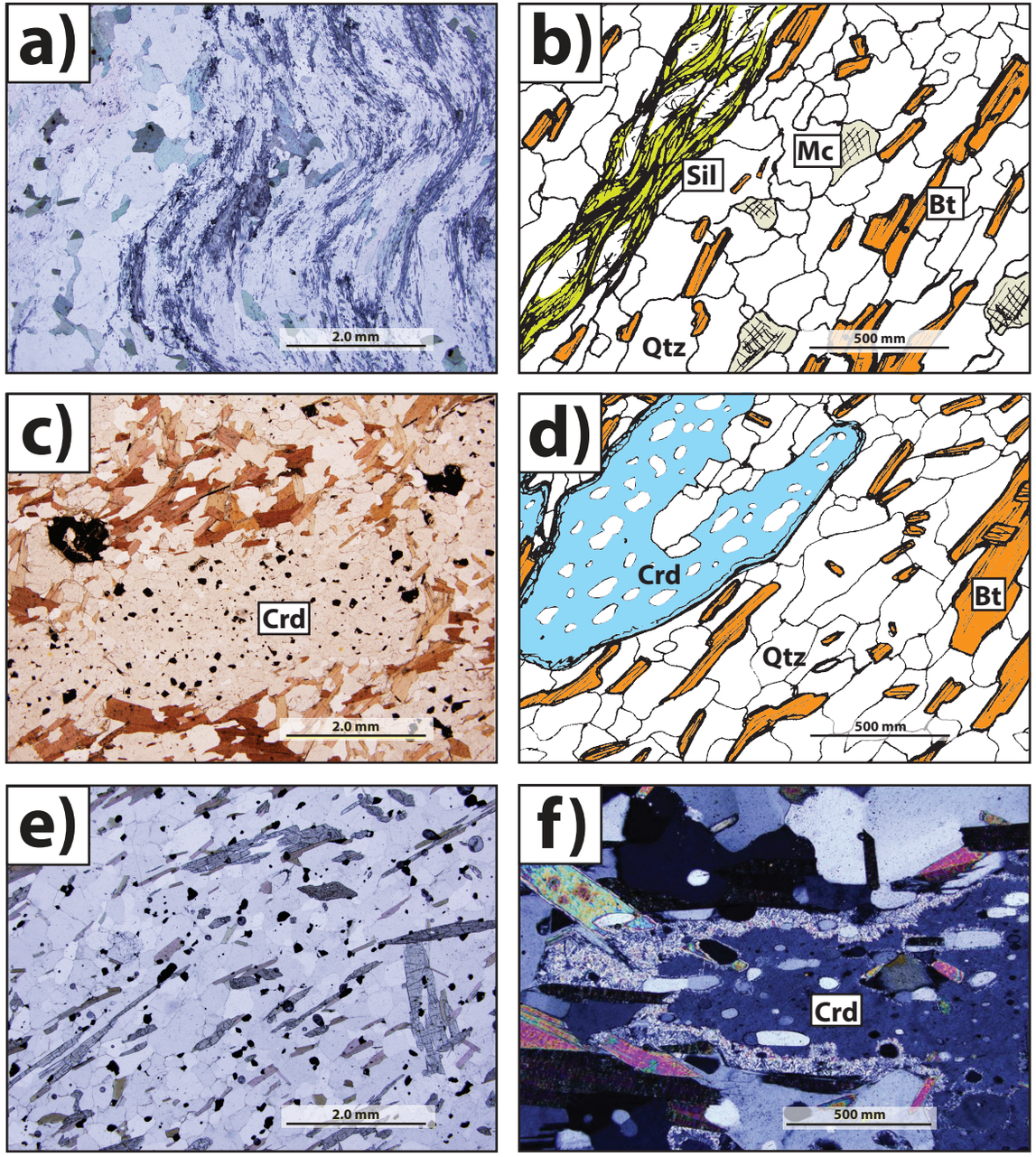
a)
2.0 mm
b)
Sil
Mc
Bt
Qtz
500 mm
c)
Crd
2.0 mm
d)
Crd
Bt
Qtz
500 mm
e)
2.0 mm
f)
Crd
500 mm

Fig. 5

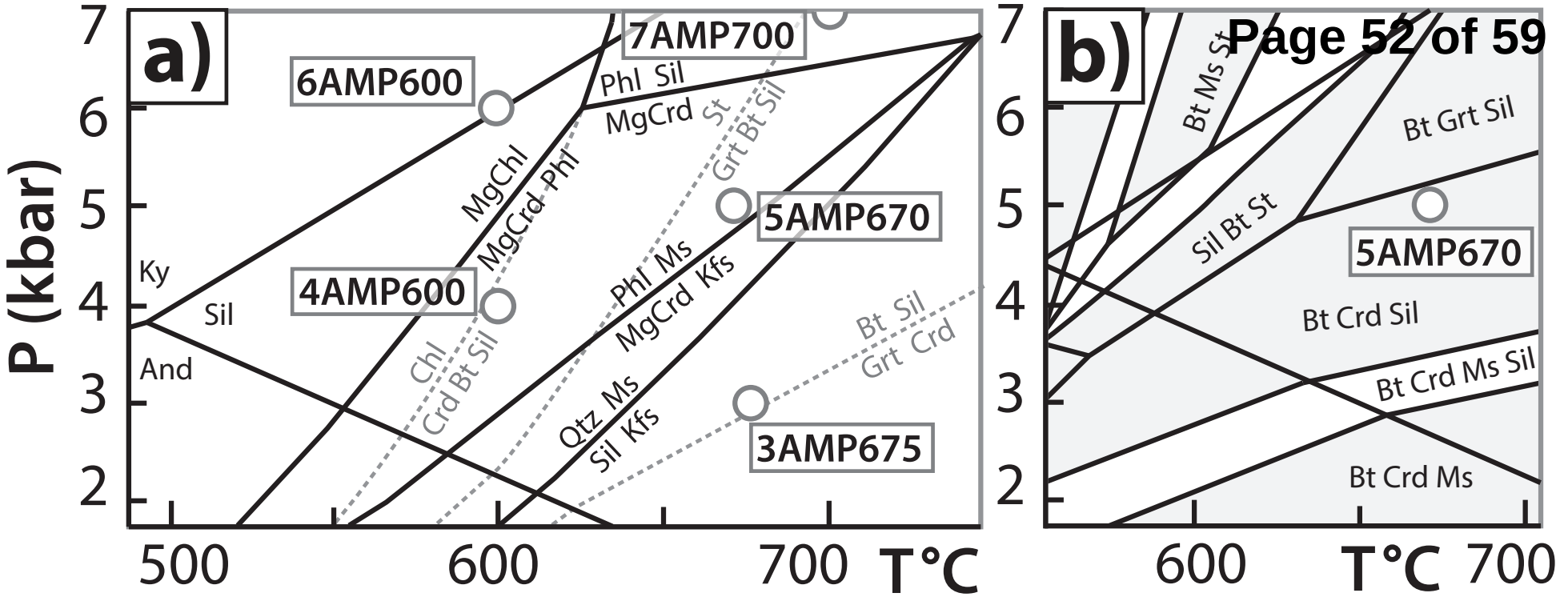
a)
6AMP600
7AMP700
5AMP670
4AMP600
3AMP675
Phl Sil
MgCrd
St
Grt Bt Sil
MgChl
MgCrd Phl
Ky
Sil
And
Phl Ms
MgCrd Kfs
Chl
Crd Bt Sil
Bt Sil
Grt Crd
Qtz Ms
Sil Kfs
P (kbar)
T°C
500
600
700
2
3
4
5
6
7
b)
Bt Ms St
Bt Grt Sil
Sil Bt St
5AMP670
Bt Crd Sil
Bt Crd Ms Sil
Bt Crd Ms
600
T°C
700

Fig. 6

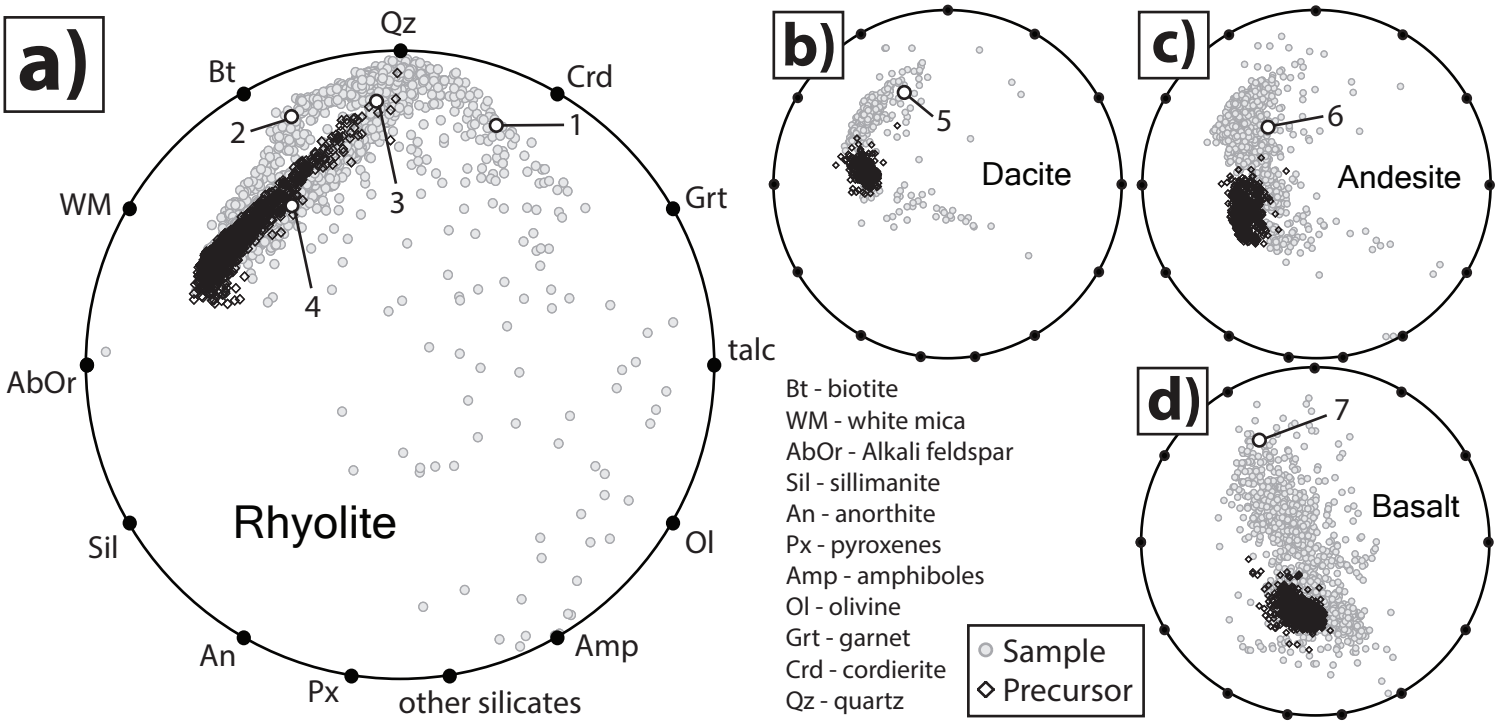
a)
Qz
Bt
Crd
2
1
WM
Grt
3
4
talc
AbOr
Rhyolite
Sil
Ol
An
Amp
Px
other silicates
b)
5
Dacite
c)
6
Andesite
d)
7
Basalt
Bt - biotite
WM - white mica
AbOr - Alkali feldspar
Sil - sillimanite
An - anorthite
Px - pyroxenes
Amp - amphiboles
Ol - olivine
Grt - garnet
Crd - cordierite
Qz - quartz
Sample
Precursor

Fig. 7

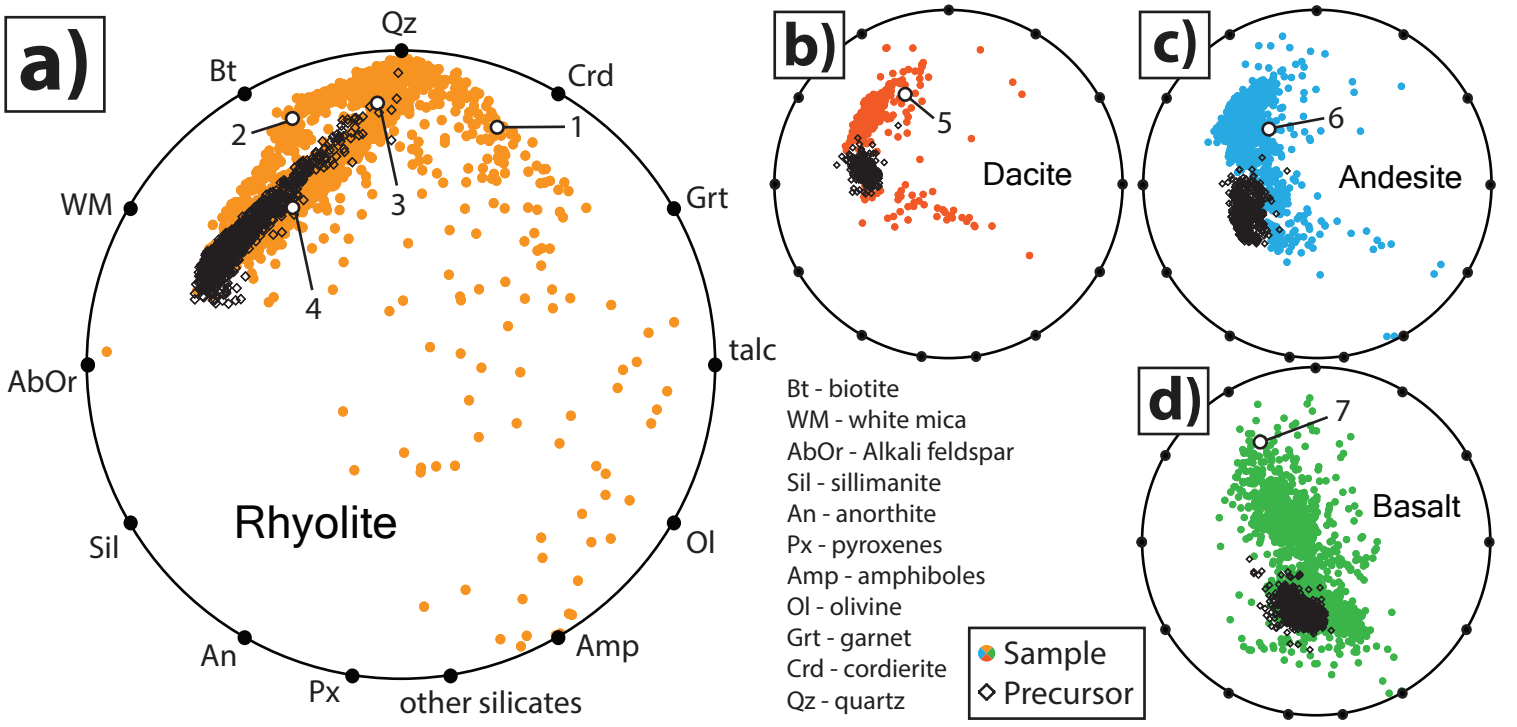
a)
Qz
Bt
Crd
2
1
WM
Grt
3
4
talc
AbOr
Rhyolite
Sil
Ol
An
Amp
Px
other silicates
b)
5
Dacite
c)
6
Andesite
d)
7
Basalt
Bt - biotite
WM - white mica
AbOr - Alkali feldspar
Sil - sillimanite
An - anorthite
Px - pyroxenes
Amp - amphiboles
Ol - olivine
Grt - garnet
Crd - cordierite
Qz - quartz
Sample
Precursor

Fig. 7

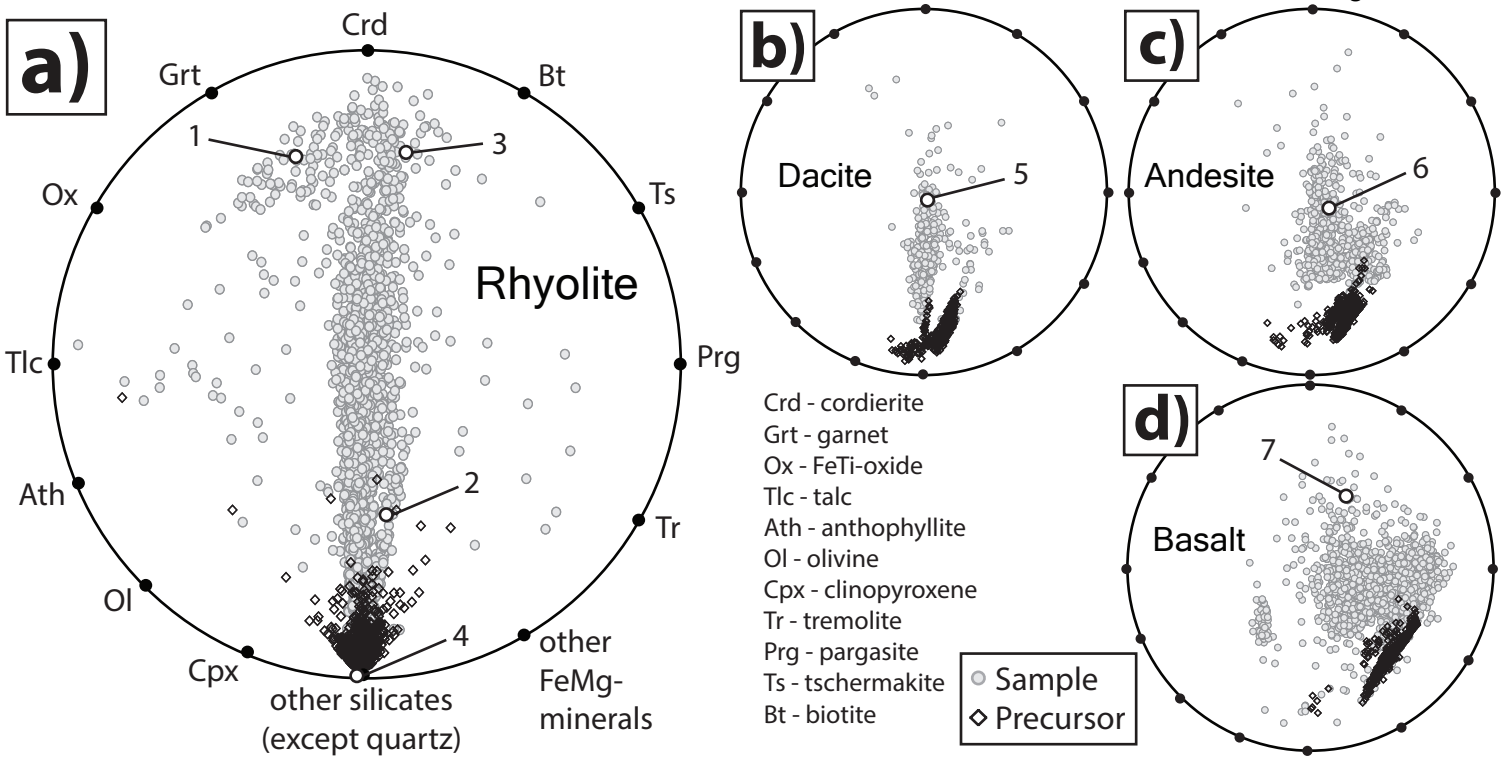
a)
Crd
Grt
Bt
Ox
Ts
Tlc
Prg
Ath
Tr
Ol
Cpx
other silicates
(except quartz)
other
FeMg-
minerals
Rhyolite
1
2
3
4
b)
Dacite
5
c)
Andesite
6
d)
Basalt
7
Crd - cordierite
Grt - garnet
Ox - FeTi-oxide
Tlc - talc
Ath - anthophyllite
Ol - olivine
Cpx - clinopyroxene
Tr - tremolite
Prg - pargasite
Ts - tschermakite
Bt - biotite
Sample
Precursor

Fig. 8

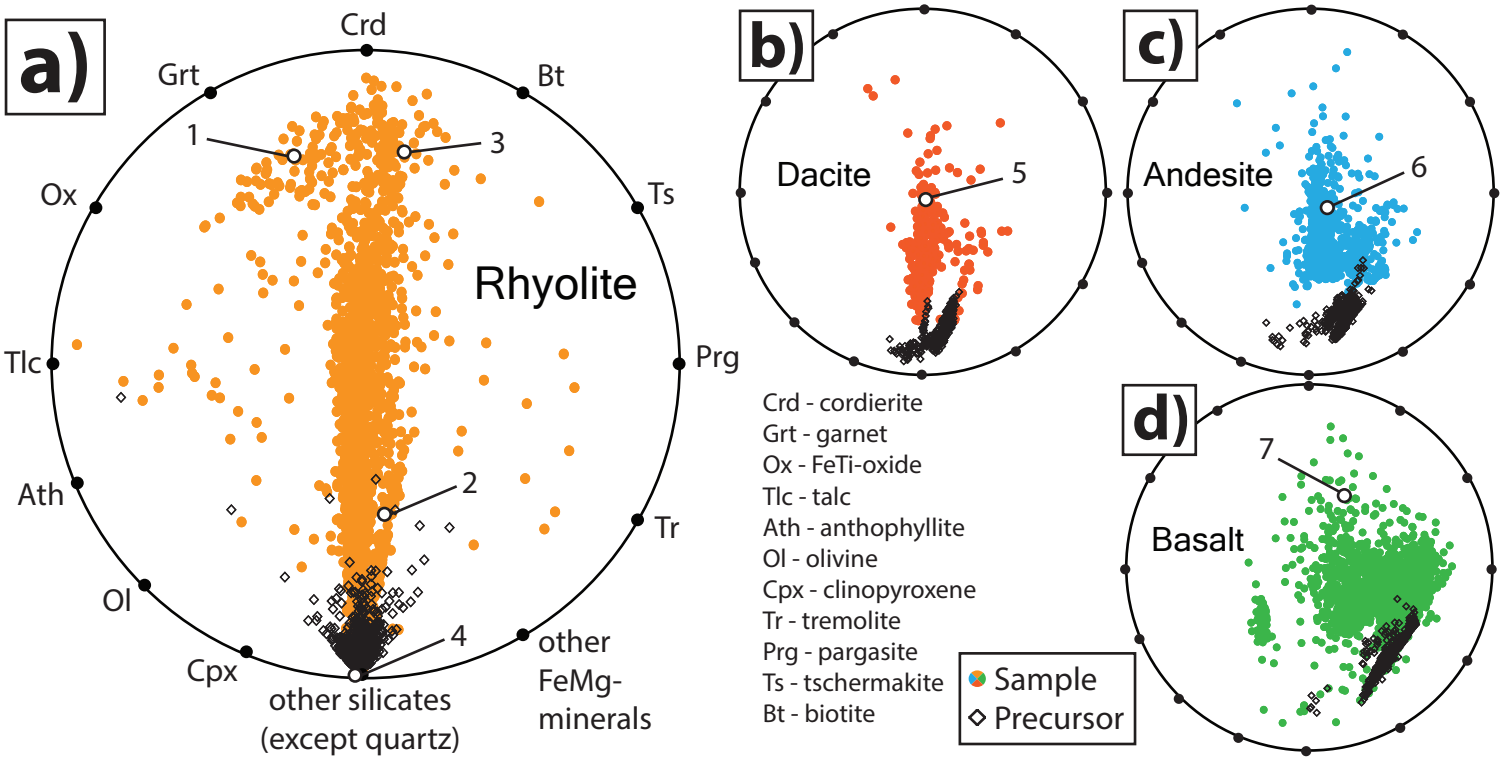
a)
Crd
Grt
Bt
Ox
Ts
Tlc
Prg
Ath
Tr
Ol
Cpx
other silicates
(except quartz)
other
FeMg-
minerals
Rhyolite
1
2
3
4
b)
Dacite
5
c)
Andesite
6
d)
Basalt
7
Crd - cordierite
Grt - garnet
Ox - FeTi-oxide
Tlc - talc
Ath - anthophyllite
Ol - olivine
Cpx - clinopyroxene
Tr - tremolite
Prg - pargasite
Ts - tschermakite
Bt - biotite
Sample
Precursor

Fig. 8

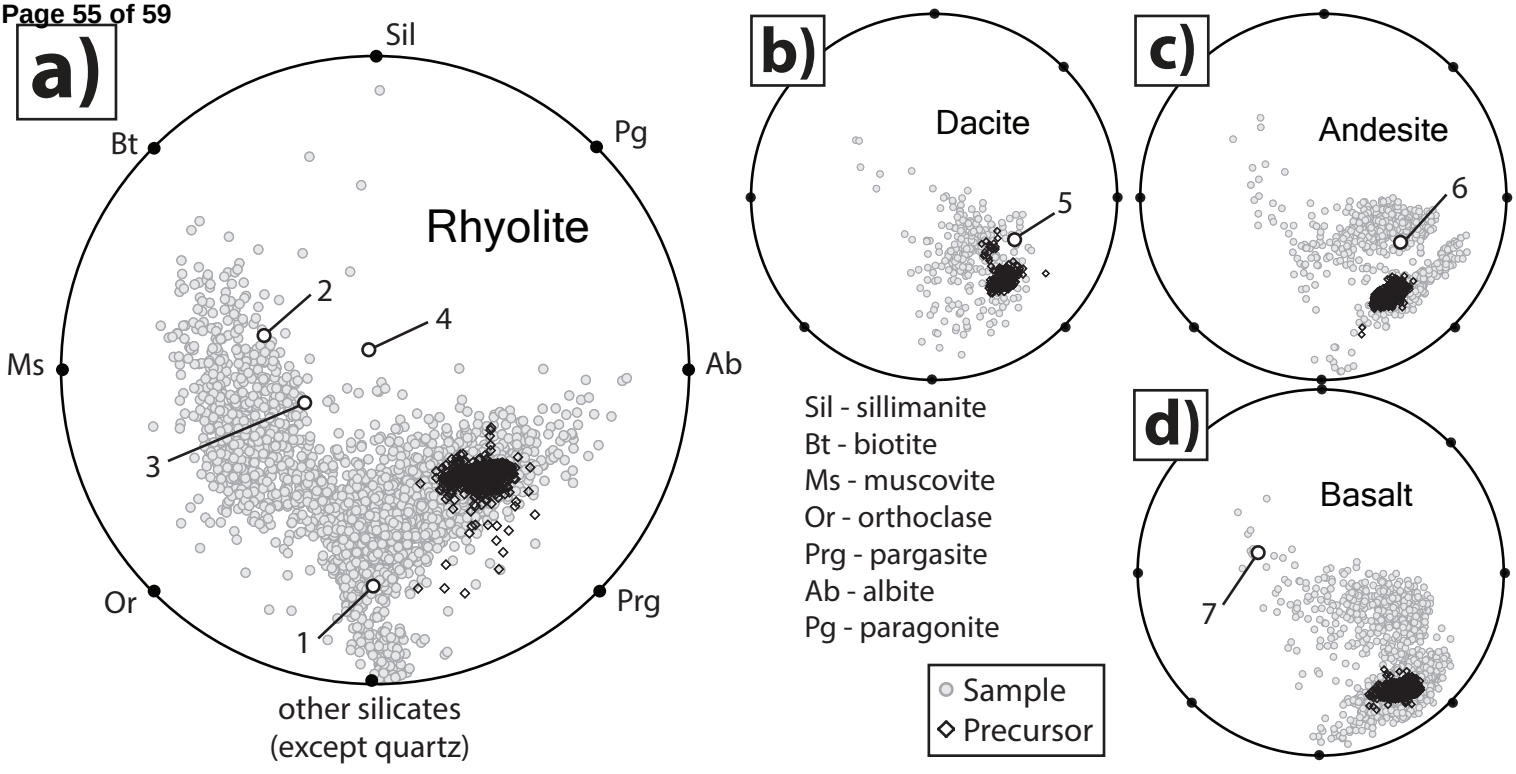
a)
Sil
Pg
Bt
Rhyolite
Ms
Ab
2
4
3
Or
Prg
1
other silicates
(except quartz)
b)
Dacite
5
c)
Andesite
6
d)
Basalt
7
Sil - sillimanite
Bt - biotite
Ms - muscovite
Or - orthoclase
Prg - pargasite
Ab - albite
Pg - paragonite
Sample
Precursor

Fig. 9

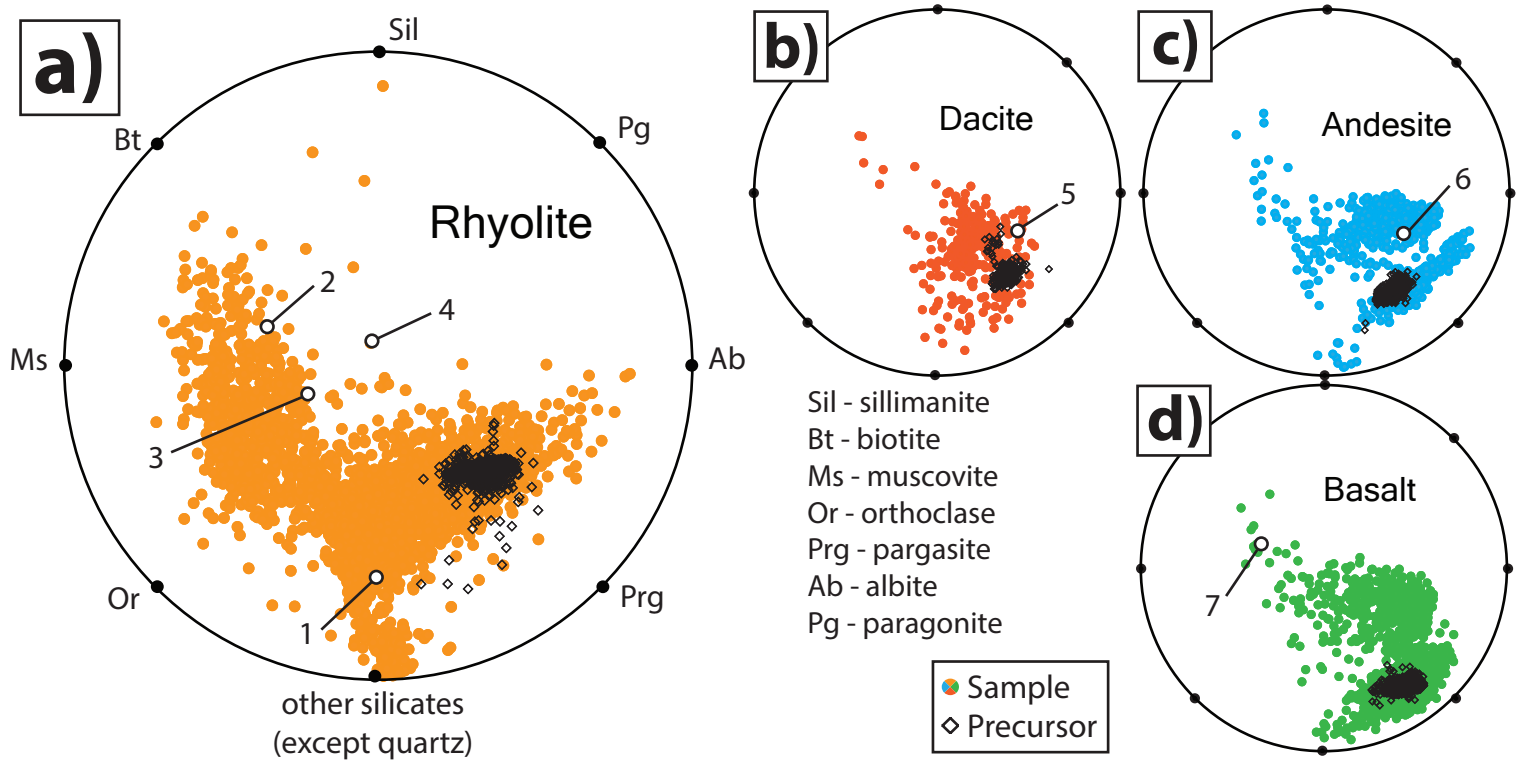
a)
Sil
Pg
Bt
Rhyolite
Ms
Ab
2
4
3
Or
Prg
1
other silicates
(except quartz)
b)
Dacite
5
c)
Andesite
6
d)
Basalt
7
Sil - sillimanite
Bt - biotite
Ms - muscovite
Or - orthoclase
Prg - pargasite
Ab - albite
Pg - paragonite
Sample
Precursor

Fig. 9

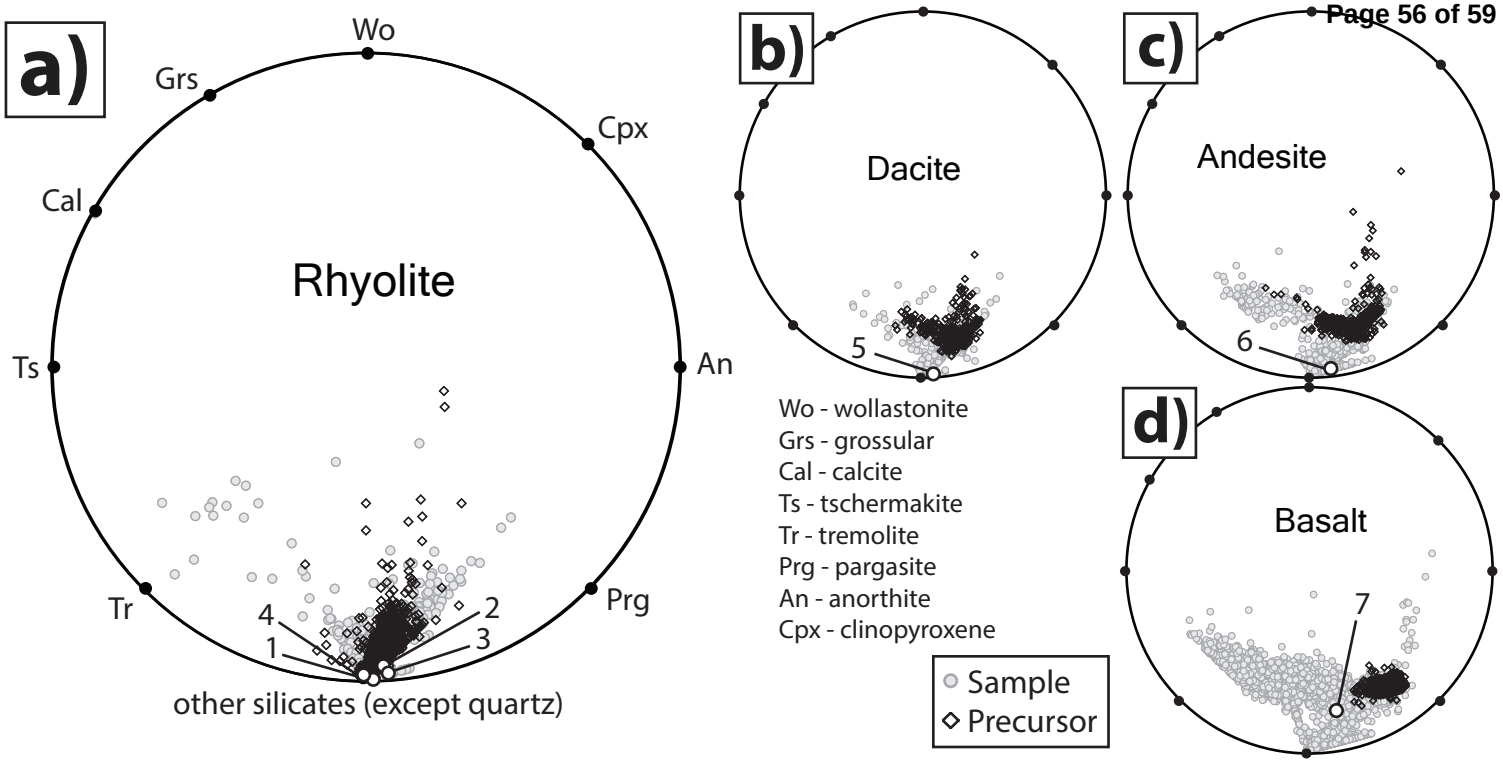
a)
Wo
Grs
Cpx
Cal
Rhyolite
Ts
An
Tr
Prg
4
2
1
3
other silicates (except quartz)
b)
Dacite
5
c)
Andesite
6
d)
Basalt
7
Wo - wollastonite
Grs - grossular
Cal - calcite
Ts - tschermakite
Tr - tremolite
Prg - pargasite
An - anorthite
Cpx - clinopyroxene
Sample
Precursor

Fig. 10

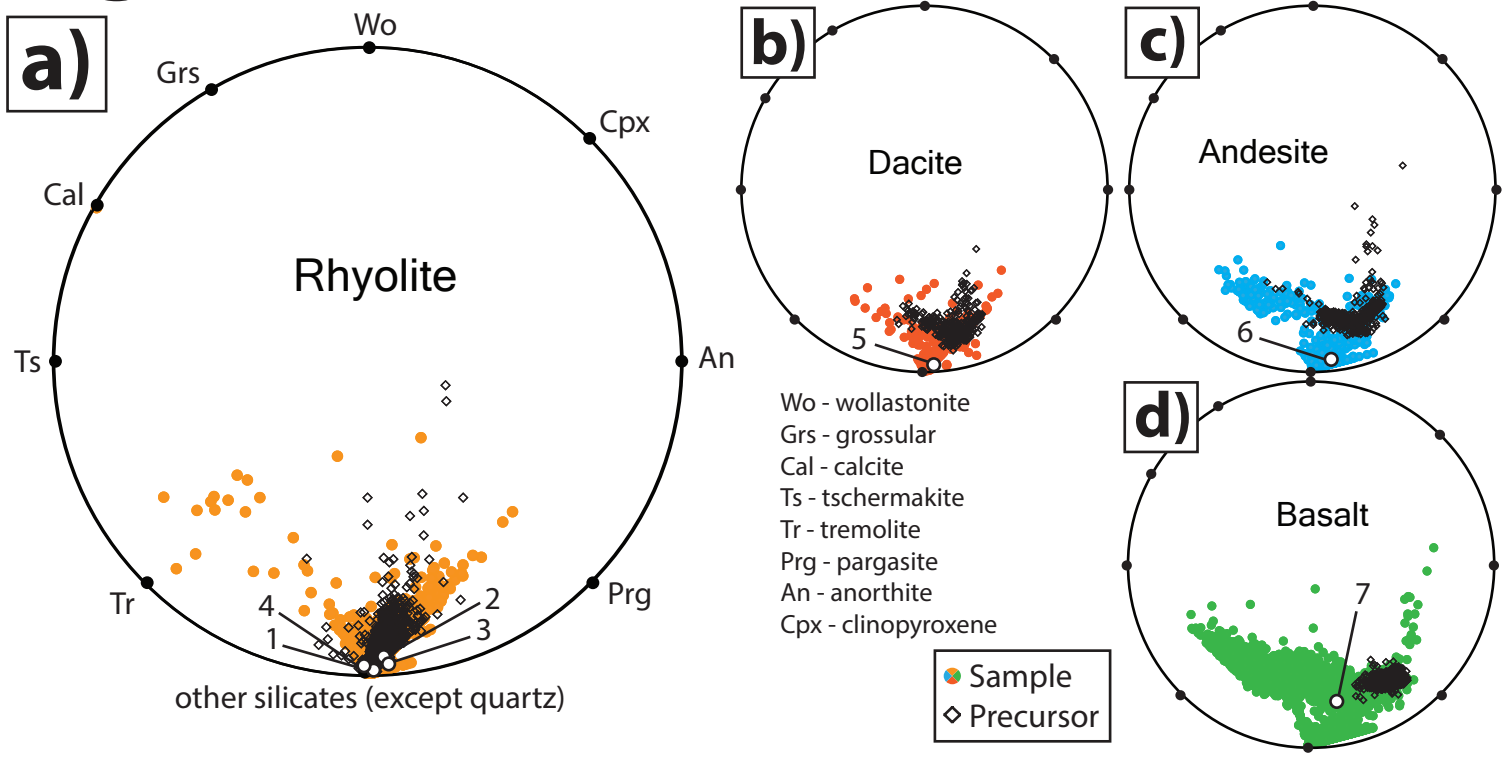
a)
Wo
Grs
Cpx
Cal
Rhyolite
Ts
An
Tr
Prg
4
2
1
3
other silicates (except quartz)
b)
Dacite
5
c)
Andesite
6
d)
Basalt
7
Wo - wollastonite
Grs - grossular
Cal - calcite
Ts - tschermakite
Tr - tremolite
Prg - pargasite
An - anorthite
Cpx - clinopyroxene
Sample
Precursor

Fig. 10

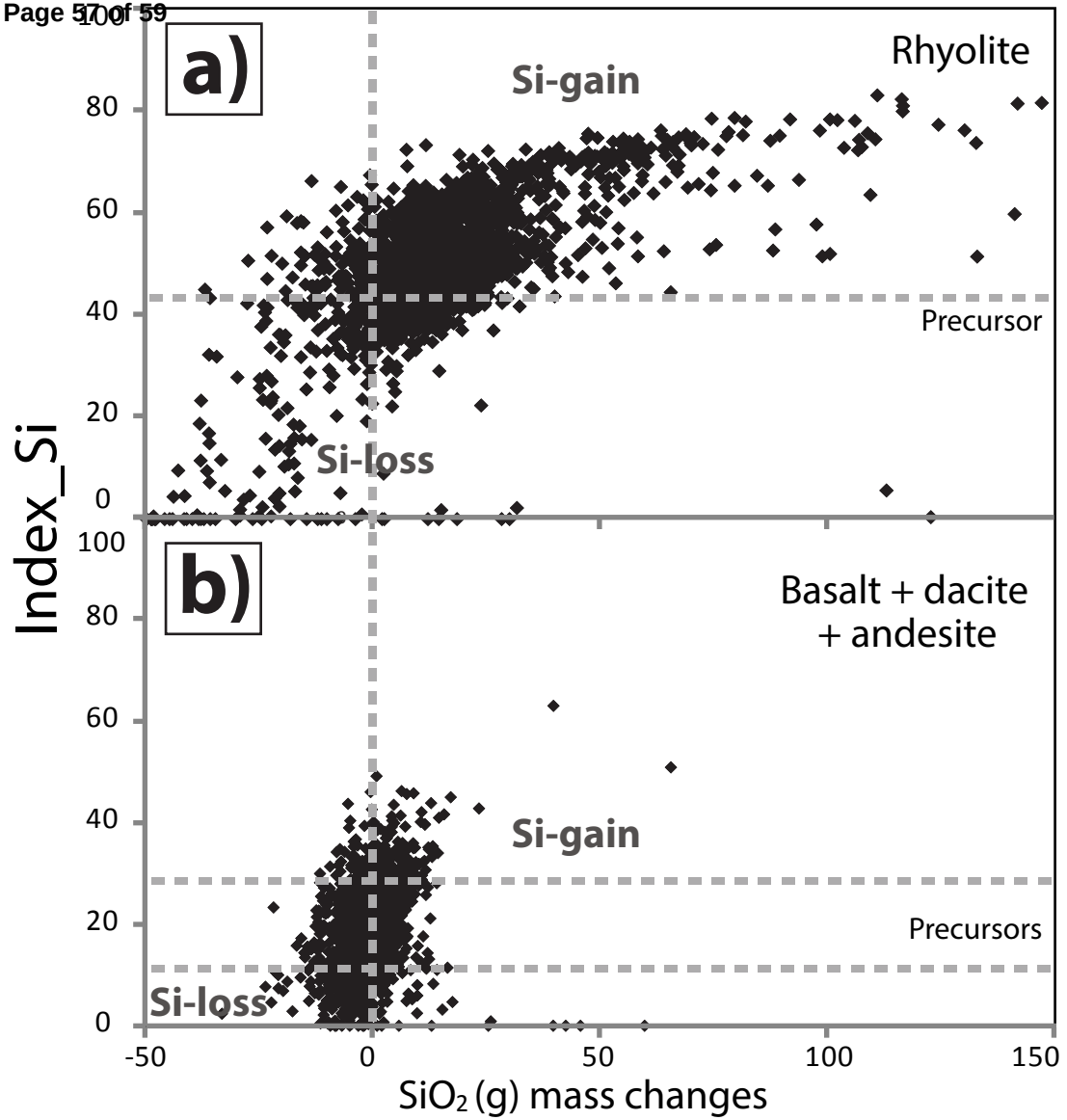
a)
Rhyolite
Si-gain
Precursor
Si-loss
b)
Basalt + dacite
+ andesite
Si-gain
Precursors
Si-loss
Index_Si
SiO2 (g) mass changes
100
80
60
40
20
0
-50
0
50
100
150

Fig. 11

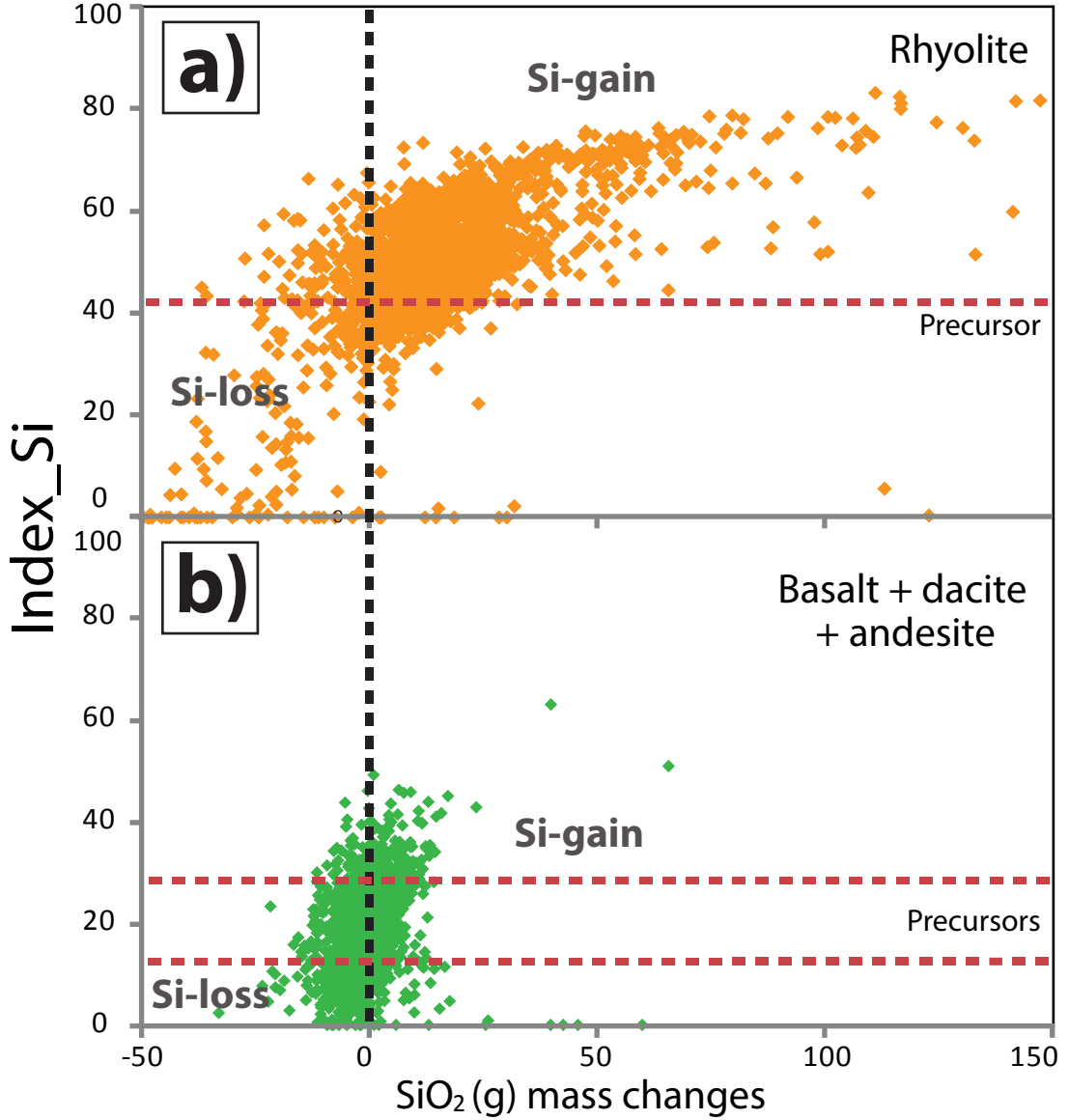
a)
Rhyolite
Si-gain
Precursor
Si-loss
b)
Basalt + dacite
+ andesite
Si-gain
Precursors
Si-loss
Index_Si
SiO2 (g) mass changes
100
80
60
40
20
0
-50
0
50
100
150

Fig. 11

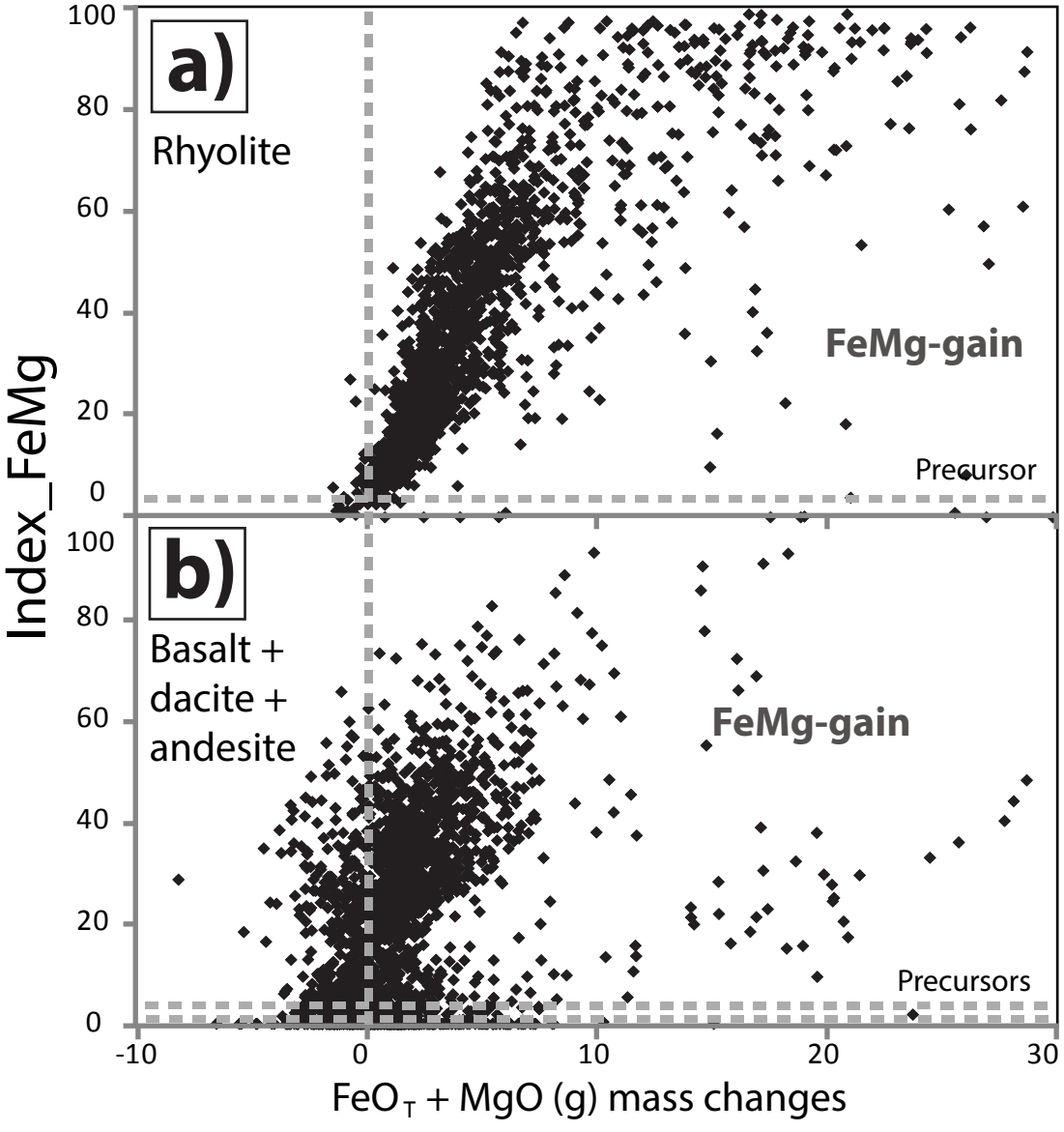
a)
Rhyolite
FeMg-gain
Precursor
b)
Basalt +
dacite +
andesite
FeMg-gain
Precursors
Index_FeMg
FeO$_T$ + MgO (g) mass changes
100
80
60
40
20
0
-10
0
10
20
30

Fig. 12

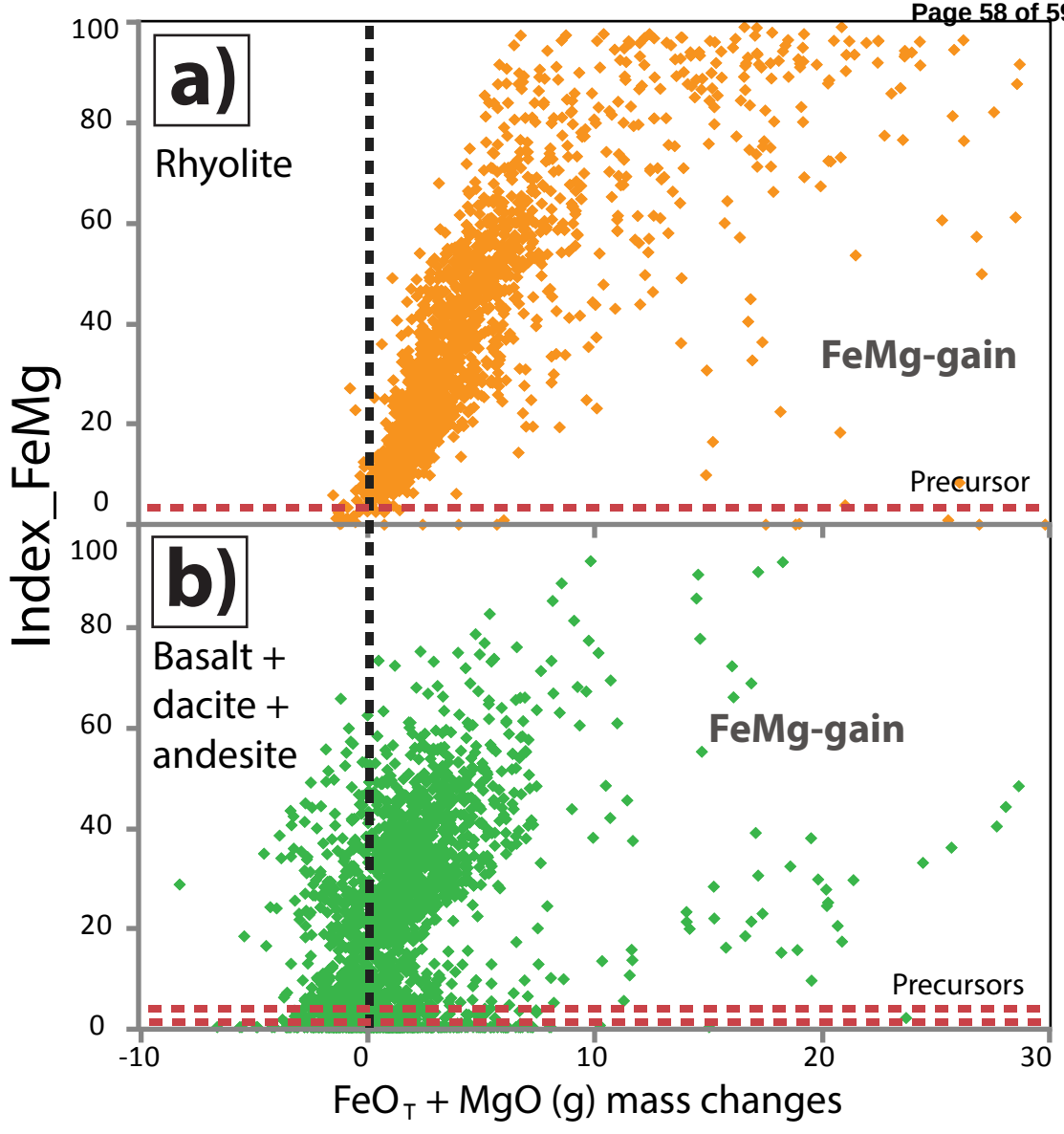
a)
Rhyolite
FeMg-gain
Precursor
b)
Basalt +
dacite +
andesite
FeMg-gain
Precursors
Index_FeMg
FeO$_T$ + MgO (g) mass changes
100
80
60
40
20
0
-10
0
10
20
30

Fig. 12

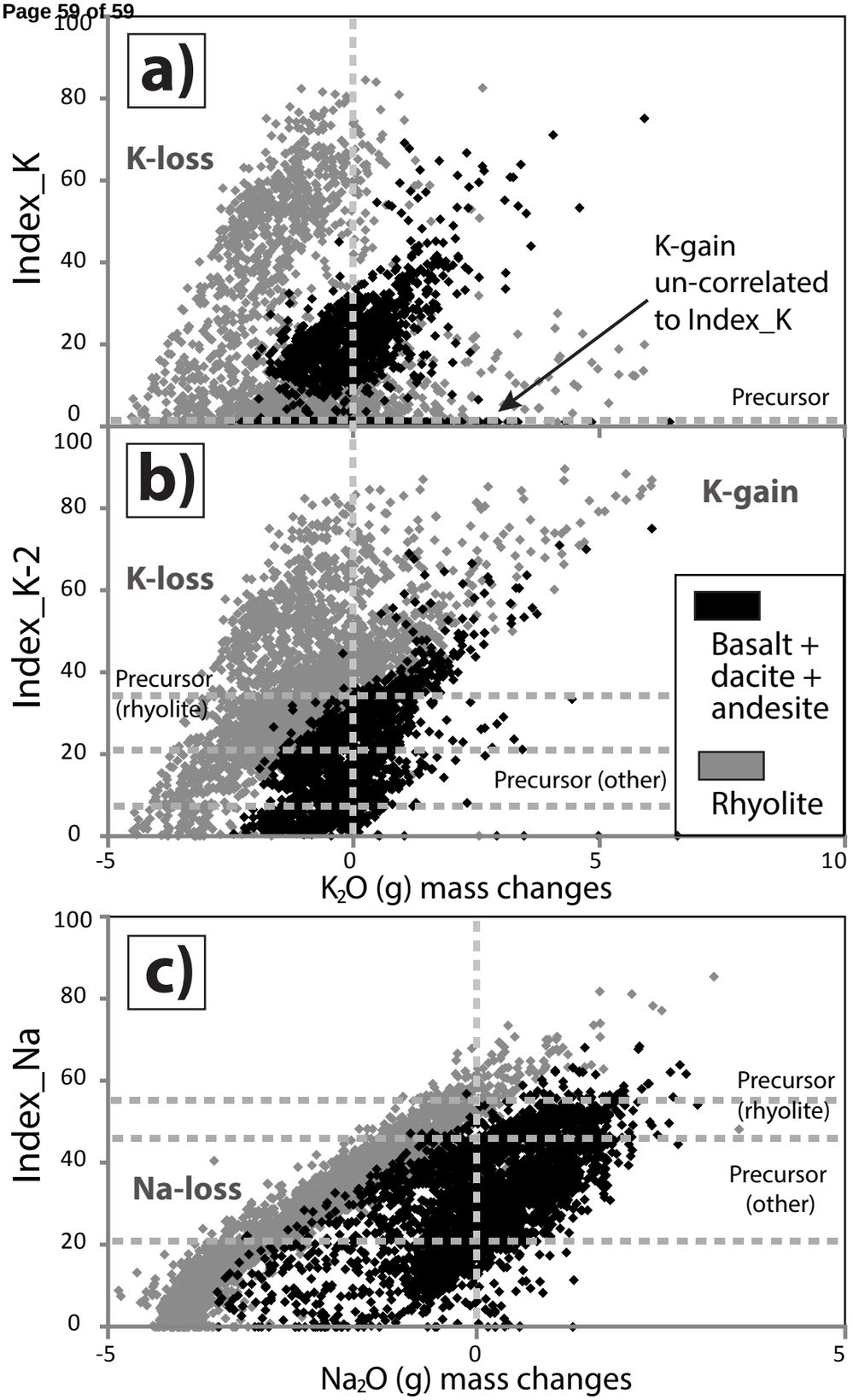
a)
K-loss
K-gain
un-correlated
to Index_K
Precursor
Index_K
b)
K-loss
K-gain
Precursor
(rhyolite)
Precursor (other)
Basalt +
dacite +
andesite
Rhyolite
Index_K-2
K_2O (g) mass changes
c)
Na-loss
Precursor
(rhyolite)
Precursor
(other)
Index_Na
Na_2O (g) mass changes

Fig. 13

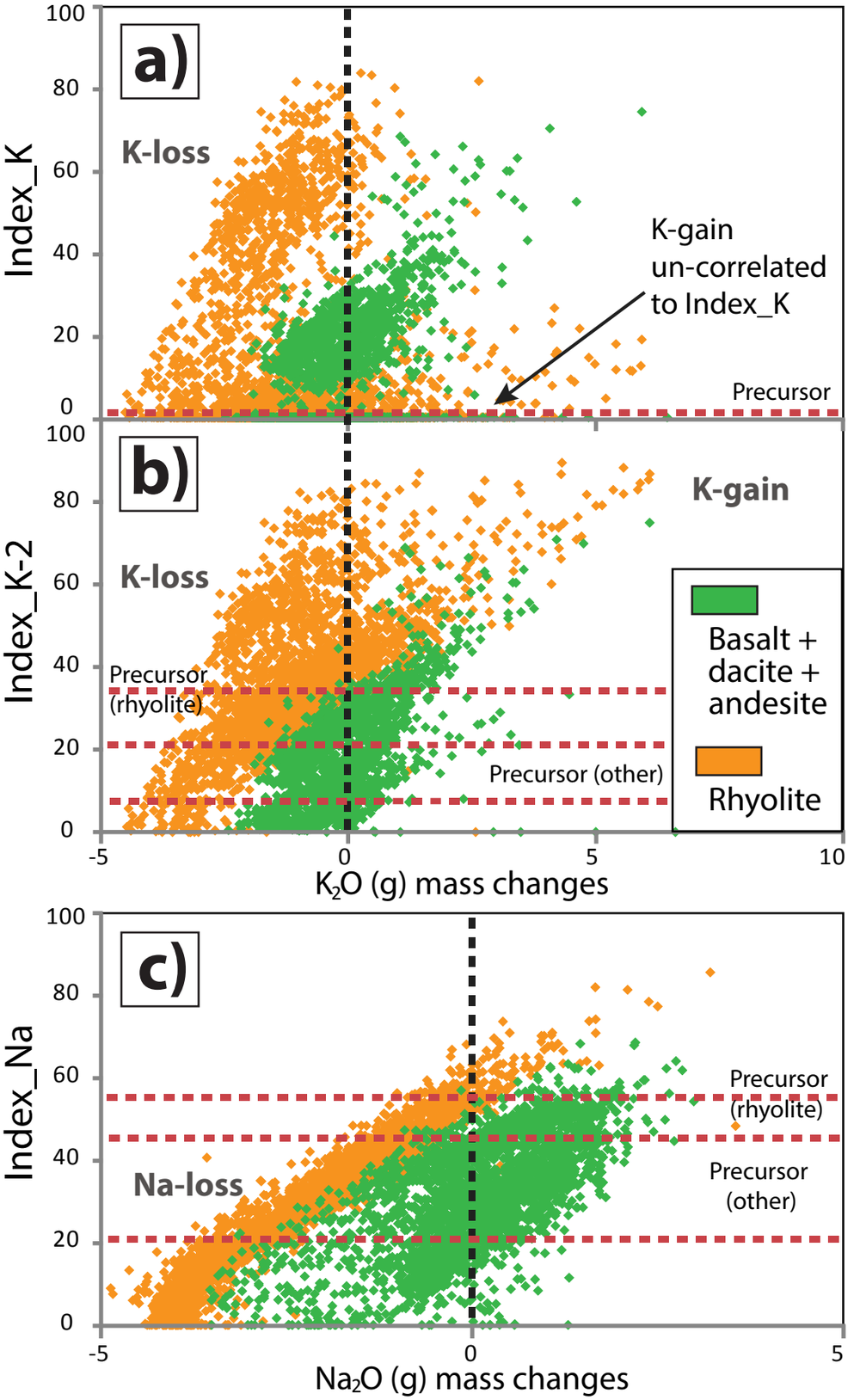
a)
K-loss
K-gain
un-correlated
to Index_K
Precursor
Index_K
b)
K-loss
K-gain
Precursor
(rhyolite)
Precursor (other)
Basalt +
dacite +
andesite
Rhyolite
Index_K-2
K_2O (g) mass changes
c)
Na-loss
Precursor
(rhyolite)
Precursor
(other)
Index_Na
Na_2O (g) mass changes

Fig. 13